

# UVM ScholarWorks

## Multiscale Expression Of Apatite Dissolution

|               |   |
|---------------|---|
| Item Type     | thesis;article  |
| Authors       | Conde, Adele  |
| Download date | 2026-05-13 10:50:53   |
| Link to Item  | <a href="https://hdl.handle.net/20.500.14849/3063">https://hdl.handle.net/20.500.14849/3063</a> |

MULTISCALE EXPRESSION OF APATITE DISSOLUTION

A Thesis Presented

By

Adele Conde

To

The Faculty of the Graduate College

of

The University of Vermont

In Partial Fulfillment of the Requirements  
For the Degree of Master of Science  
Specializing in Geology

August, 2019

Defense Date: June 28, 2019

Thesis Examination Committee:

Nicolas Perdrial, Ph.D., Advisor

Ehsan Ghazanfari, Ph.D., Chairperson

John M. Hughes, Ph.D.

Roland Hellmann, Ph.D.

Cynthia J. Forehand, Ph.D., Dean of the Graduate College

## Abstract

The weathering of apatite is the foundation of the phosphorus cycle and essential to life, yet little is known about the nanoscale mechanisms driving apatite weathering. Deciphering nanoscale dissolution in apatite is a significant step to understand phosphate weathering behavior, that was key to the development of life. Determining what controls apatite weathering can impact many areas of environmental and medical mineralogy such as dentistry, contaminant scavenging, geochronology, and paleoenvironment studies. The aim of this study was to characterize apatite dissolution across scales with an emphasis on the nanoscale mechanisms. Recent research on the weathering of silicate minerals at the nanoscale has provided telling evidence of a relatively new chemical weathering model referred to as coupled interfacial dissolution-precipitation (CIDR) mechanism. We hypothesize that this mechanism could be broadened to phosphate minerals.

To investigate crystals of Durango fluorapatite (FAP) and hydroxyl-chlorapatite (HAP) were hydrolyzed in flow-through devices with pH 3 HNO<sub>3</sub> solutions. Apatites used in the study were chemically and structurally characterized via Single Crystal-XRD, with particular emphasis on the anion composition and atomic arrangement. Determination of the mechanisms of dissolution was carried at multiple scales using ICP-OES chemical analysis (macroscale), SEM (microscale) and STEM-HAADF-EDS/EELS on FIB liftouts (nanoscale).

At the macroscale, The anionic composition of the apatite controlled its weathering rate. As expected, HAP dissolution occurred at faster rates compared to FAP. SEM characterization of the crystal surfaces pre- and post-dissolution revealed the development of etch pits during dissolution, however, more pronounced for FAP than HAP. Observation of the mineral/solution interface at the nanoscale using STEM-HAADF revealed the development of a nanometric amorphous layer likely depleted in Ca compared to P.

The observation of a sharp crystalline/amorphous transition and 5 to 15 nanometers thick amorphous surface altered layer, associated with a depletion in Ca suggests that similar to silicate, apatite is subject to a coupled interfacial dissolution-reprecipitation mechanism. This potential discovery could transform our understanding of phosphate behavior in medical and environmental mineralogy fields.

## Acknowledgements

I would like to thank the following people and organizations of their support during graduate career, without which I would not have been able to complete this work. My advisor Nico Perdrial for his guidance and encouragement. The UVM Geology Department for being my home for the past two years. Roland Hellman for always offering a helping hand and sharing his knowledge and expertise with me. John Hughes, my go to expert on apatite, for his help conducting Single Crystal XRD and always having a fun scientific fact to share. Ehsan Ghazanfari for his support serving as my committee Chair. Stephen Wright for dragging me out of my office rain, shine, or snow for the sake of glacial land forms and bakeries.

The Vermont NASA National Space Grant College and Fellowship Program and GSA Graduate Research Grant for their support and funding of my research. Nanoeath at Virginia Tech, specifically, Marc Michel for providing a mixed flow reactor for dissolution experiments, Mitsu for his help preparing fluorapatite FIB liftouts and conducting HTEM/EELS analysis. Liz Rampe, Roy Christoffersen and ARES Division at Johnson Space Center for their help preparing hydroxyapatite FIB liftouts and conducting HRTEM/EDS analysis.

Finally, I would like to thank my family. My parents Kevin and Georgene for their unwavering support and encouragement. My four older siblings Andrea, Robert, Nica, and Maggie for sharing their wisdom with me and always watching out for me. My four nieces Elinor, Olivia, Cecily, and Lydia for making me laugh and unknowingly encouraging me to be the best I can be. I would also like to thank my boyfriend Ryan for his encouragement, support, and proof-reading skills.

## Table of Contents

|  |     |
|--|-----|
| Acknowledgements.....  | ii  |
| Table of Contents.....   | iii |
| List of Tables .....   | v   |
| List of Tables .....   | vi  |
| Chapter 1: Introduction and Comprehensive Literature Review .....  | 1   |
| 1.1 Introduction .....   | 1   |
| 1.2 Dissolution Mechanisms in Silicates.....   | 3   |
| 1.2.1 Leached Layer Model vs. Coupled Interfacial Dissolution Reprecipitation (CIDR) Model .....                                 | 3   |
| 1.2.2 Recent Evidence of the CIDR Model.....   | 5   |
| 1.3 Chemical Structure and Weathering Behavior of Apatite.....   | 6   |
| 1.4 Implications of a Nanoscale Dissolution-Reprecipitation Mechanism in Apatite .....   | 7   |
| 1.5 References Cited .....   | 9   |
| Chapter 2: Chemical and Structural Characterization of Apatite: The Role of Anions and Implication for Weathering Behavior ..... | 15  |
| 2.1 Introduction .....   | 15  |
| 2.2 Material and Methods.....  | 17  |
| 2.2.1 Apatite Specimens.....   | 17  |
| 2.2.2 Single Crystal XRD.....  | 18  |
| 2.2.3 Bond Valence Calculations.....   | 19  |
| 2.3 Results and Discussion .....   | 19  |
| 2.3.1 Fluorapatite.....  | 20  |
| 2.3.2 Hydroxyl-chlorapatite .....  | 22  |

|   |    |
|---|----|
| 2.3.3 Effect of Anion Column Arrangement and Bond Distances ..... | 27 |
| 2.3.4 Implications for Weathering Behavior .....                  | 27 |
| 2.4 Conclusion .....  | 30 |
| 2.5 References Cited .....  | 31 |
| Chapter 3: Multiscale Expression of Apatite Dissolution.....      | 34 |
| 3.1 Introduction .....  | 34 |
| 3.2 Material and Methods .....                                    | 36 |
| 3.2.1 Apatite Characterization.....                               | 36 |
| 3.2.2 Dissolution Experiments .....                               | 36 |
| 3.2.3 Dissolution Rate and Degree of Undersaturation.....         | 38 |
| 3.2.4 SEM and FIB-TEM Analysis.....                               | 39 |
| 3.3 Results .....   | 40 |
| 3.3.1 Macroscale.....   | 40 |
| 3.3.2 Microscale .....  | 41 |
| 3.3.3 Nanoscale .....   | 43 |
| 3.4 Discussion .....  | 46 |
| 3.5 Conclusion and Implications.....                              | 49 |
| 3.6 References Cited .....  | 51 |
| Chapter 4: Conclusions.....                                       | 58 |
| Chapter 5: Bibliography.....                                      | 60 |
| Appendix A: Detailed HRTEM/EDX and EELS Methods.....              | 69 |

## List of Tables

|   |    |
|---|----|
| Table 2-1. Atomic coordinates and equivalent isotropic atomic displacement parameters ( $\text{\AA}^2$ ) for Durango fluorapatite. ....         | 21 |
| Table 2-2. Value of z for column anions in (0,0,z) sites and percentage of total anion occupancy in Durango fluorapatite. ....                  | 21 |
| Table 2-3. Atomic coordinates and equivalent isotropic atomic displacement parameters ( $\text{\AA}^2$ ) for natural hydroxyl-chlorapatite..... | 23 |
| Table 2-4. Value of z for column anions in (0,0,z) sites and percentage of total anion occupancy in natural hydroxyl-chlorapatite. ....         | 23 |
| Table 2-5. Bond lengths between Ca2 atoms and column anions. ....   | 29 |

## List of Figures

|  |    |
|--|----|
| Figure 1-1. Comparison of silicate dissolution mechanisms a) Formation of the SAL according to a) the leach layer model b) the CIDR model. Both views are cross-sections with arbitrary scales. (Modified from Hellmann et al. et al 2012). .....  | 4  |
| Figure 1-2 HRTEM image of the interface between unaltered wollastonite and the surface altered layer, with insert showing EFTEM Si and Ca profiles taken along the A-B transverse (from Hellmann et al. 2012).....   | 5  |
| Figure 2-1. Crystal structure of apatite looking down the C axis. ....   | 16 |
| Figure 2-2. Euhedral crystals of a) Durango fluorapatite and b) hydroxyl-chlorapatite ground for single crystal-XRD.....   | 18 |
| Figure 2-3. Depiction of the anion column reversal, necessary to maintain symmetry and remain in space group $P6_3/m$ , with an acceptable sequence of atom in Durango fluorapatite. ....  | 21 |
| Figure 2-4. Disorder of $Ca_2$ to $Ca_2'$ to accommodate Cl in the ClOH site. ....   | 23 |
| Figure 2-5. Depiction of the anion column reversal, necessary to maintain symmetry and remain in space group $P6_3/m$ , with an acceptable sequence of atoms in Hydroxyl-chlorapatite. ....  | 26 |
| Figure 3-1. Experimental set up of dissolution experiments. ....   | 38 |
| Figure 3-2. Evidence of surface alteration post-weathering by comparing unaltered a) HAP and b) FAP with weathered c) HAP and d) FAP.....  | 41 |
| Figure 3-3. Evolution of average HAP and FAP Ca-based dissolution rates ( $\log R_{Ca}$ ( $\text{mol m}^{-2} \text{s}^{-1}$ )) as a function of time. b) FAP and c) HAP pH and ratio of dissolved Ca and P throughout weathering of individual experiments. The influent solution was pH 2.95 for FAP and 3.04 for HAP at time = 0 and increased to 3.1 and 3.3 respectively. The red line represents the stoichiometric ratio (1.67) based on the bulk apatite composition. Both FAP and HAP appear preferentially released Ca compared to P in the first 24 to 48 hours of reaction before becoming stoichiometric as the system reached dynamic steady-state dissolution..... | 42 |
| Figure 3-4. SEM images of $10\bar{1}0$ faces of FAP a) before and b) after weathering with detail insert and HAP c) before and d) after weathering .....   | 43 |

Figure 3-5. a) and b) Cross-sectional HRTEM images of HAP showing a nanometric sharp boundary between the unaltered HAP (white) and an amorphous SAL (yellow) and a protective coating of carbon (black). Both images were taken on the same FIB prepared cross-section milled perpendicular to the  $10\bar{1}0$  face. c) and d) EDS Elemental Maps of Ca and P and e) extracted line profile of Ca, P, and O created from EDS compositional spectrum images. .... 44

Figure 3-6. a) HRTEM image of the crystal surface of weathered FAP and corresponding SAED patterns. Unaltered, altered and coated layers are identified in the lower end of the image. b) and c) Darkfield HAADF-TEM images of location of EELS Profiles taken along A-A' and B-B' transects (red lines). d) EELS chemical profiles corresponding to A-A' and B-B' transects (red lines) across the interface between the SAL and the unaltered FAP and Ca to P electron intensity ratio across the transect B-B'. .... 45

## **Chapter 1: Comprehensive Literature Review**

### **1.1 Introduction**

Phosphate minerals have a disproportionate importance relative to other mineral classes. Largely in part because phosphorus is required for life to occur, as a significant component of our DNA, ATP, and RNA (Adcock et al. 2013; Pasek and Kee, 2011), but also its environmental impact (Oelkers and Valsami-Jones, 2008). Apatite is the most abundant phosphate mineral, and its weathering is the primary source of phosphorus (P) in the environment (Filippelli, 2008), and likely played a crucial role in P availability necessary for the development of life (Schwartz 2006; Powner et al. 2009). Unlike other macronutrients, P has no primary volatile phase, remaining in phosphate minerals until weathering releases it into the environment (Filippelli, 2002). P is so essential to life; it is often the most biologically limiting factor in an ecosystem (Chadwick et al. 1990).

These macroscale expressions of weathering reactions have been fundamental to the development of life and are critical in its conservation and evolution. It has also been shown that micro- to nanoscale conditions are the controlling factor of mineral weathering (Banfield et al. 1991; Maher et al. 2006; Noiriel et al. 2012), suggesting that small-scale processes have significant implications for macroscale processes. Many studies have even suggested that the solution to the longstanding discrepancies between mineral dissolution rates measured in the field and laboratory experiments lies in a complete understanding of nanoscale and molecular scale weathering processes (Maher et al. 2006; Steefel et al. 2015; White and Brantley, 2003).

Furthermore, Steefel et al. (2005) state the ultimate test of understanding in the field of geochemistry is the ability to predict all geochemical processes, no matter how small. These studies, in addition to the need to understand the role of mineral weathering

in large-scale geochemical cycles, demonstrate that it is of the utmost importance to investigate these small-scale processes. Recent research on the nanoscale mechanisms driving the dissolution of silicate minerals and glasses is revolutionizing our understanding of weathering and helping to resolve these questions.

Recent advances in sub-nanoscale chemical and structural imaging, such as Atom Probe Tomography and developments in High-Resolution Transmission Electron Microscopy, are now allowing scientists to assess mineral dissolution mechanisms at the nanoscale, leading to the reevaluation of the traditional leached layer model concept of mineral dissolution. As a result, compelling new evidence suggests a relatively new chemical dissolution mechanism referred to as coupled interfacial dissolution-precipitation, (CIDR - Hellmann et al. 2015; Hellmann et al. 2012, Hellmann et al. 2003, Putnis and Ruiz-Agudo et al. 2016; Putnis and Ruiz-Agudo et al. 2013). Although the CIDR model was conceptually introduced by Taylor and O'Neil (1967), there were no analytical methods available to evaluate its validity.

While the consensus is shifting toward CIDR as a dissolution mechanism for silicate minerals (Cappelli et al. 2015; Grant et al. 2014; Putnis, 2014; Reis, 2015; Ruiz-Agudo et al. 2014, 2016; Steefel et al. 2015), to-date no similar investigation has been performed on non-silicate minerals. A potential extension of the CIDR theory to mineral families other than silicates, such as phosphate minerals, would imply a paradigm shift in the conceptual framework of one of Earth most essential processes: the weathering of rock and minerals.

## 1.2 Dissolution Mechanisms in Silicates

### 1.2.1 Leached Layer Model vs. Coupled Interfacial Dissolution-Reprecipitation (CIDR) Model

Silicate dissolution experiments performed in acidic conditions consistently show an initial non-stoichiometric, apparent release of interstitial cations and Al, resulting in the formation of a chemically distinct surface altered layer (SAL) also referred to as the "leached layer". This observation can be explained by two contradicting theories, the leached layer model or the CIDR model.

The leach layer model suggests the mechanism responsible for the formation of this leached layer is the result of two different processes occurring simultaneously: (1) Solid-state interdiffusion of interstitial cations from the mineral and protons from the bulk solution and (2) hydrolysis reactions that remove silicon and oxygen from the leached layer and release it into the bulk solution (Fig. 1-1a - Casey et al. 1988, 1993; Hellmann, 1994, 1995; Muir et al. 1989, 1990; Petit et al. 1989; Schweda et al. 1997).

Alternatively, The CIDR model suggests the mechanism responsible for the formation of this SAL is the result of three different processes occurring simultaneously: (1) Congruent dissolution occurs on a single reaction front in a thin fluid film at the interface between the altered layer and the pristine mineral allowing all atoms to be released at the same stoichiometric rate; (2) a surface altered layer is formed by coupled reprecipitation of a distinct porous and amorphous phase; and (3) this reprecipitation occurs as an interfacial process, distinct from traditional precipitation from a bulk solution that is oversaturated (Fig. 1-1b - Hellmann et al. 2012).

A major expected difference between the respective models is the concentration change in interstitial cations through the SAL or leached layer. If dissolution occurs by

solid-state interdiffusion, as suggested by the leach layer model, a sigmoidal concentration gradient of interstitial cations is expected to form within the leached layer, where the concentration decrease occurs throughout the entire layer (dashed profiles, figure 1-1a). If the SAL forms by means of the CIDR model a sharp nanometric decrease or “break” in the concentration of interstitial cations is expected at the interface between the pristine mineral and the SAL (dashed profiles, figure 1-1b).

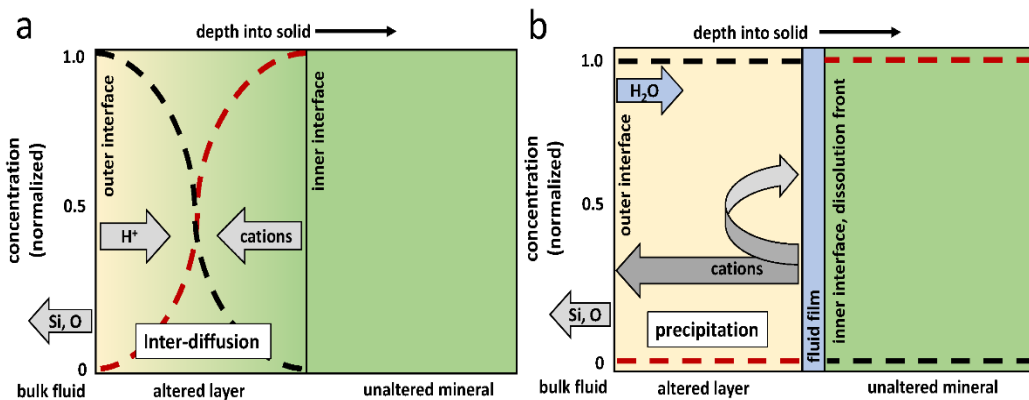
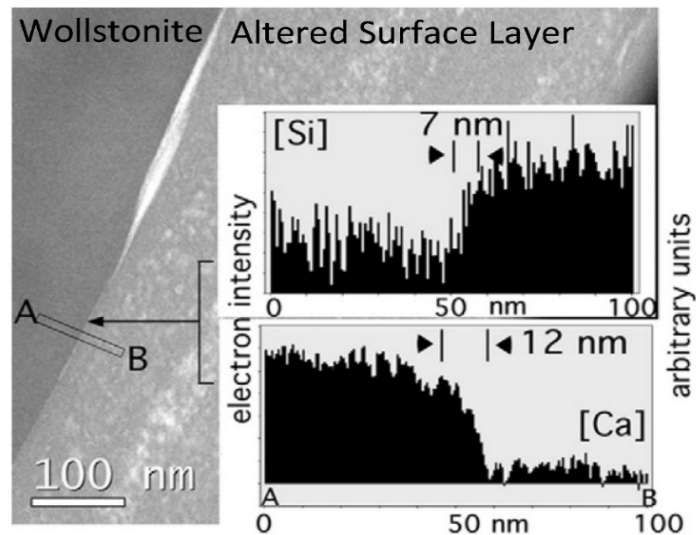


Figure 1-1. Comparison of silicate dissolution models a) Formation of the SAL according to a) the leach layer model b) the CIDR model. Both views are cross-sections with arbitrary scales. (Modified from Hellmann et al. 2012).

The CIDR model was first suggested for silicate mineral replacement in hydrothermal environments as an alternative to solid-state diffusion by O'Neil and Taylor (1967). However, this model remained unsubstantiated until recently due to spatially inadequate analytical techniques for characterizing the SAL or leached layer. Advances in sub-nanoscale chemical and structural imaging, mass spectrometry, and spectroscopy are now allowing scientists to investigate dissolution mechanisms in silicate minerals at a higher spatial resolution than ever before. Recent experiments and analyses of weathered silicate minerals and glasses have provided evidence for a nanoscale CIDR mechanism (Geisler et al. 2010, 2015; Hellmann et al. 2003, 2012, 2015; Putnis, 2002, 2009, 2014; Putnis and Putnis, 2007; Ruiz-Agudo et al. 2012, 2014).

### 1.2.2 Recent Evidence of the CIDR mechanism

In two seminal papers, (Hellmann et al. 2003; 2012) demonstrated that a variety of structurally diverse silicate minerals (single chain inosilicates: diopside and wollastonite, nesosilicates: pyrope garnet and olivine, and a plagioclase feldspar series: albite, labradorite, and anorthite) form a surface altered layer that consists of a homogeneous, porous, amorphous, Si-rich and interstitial cation-depleted material with a spatially nm-sharp structural and chemical interface (Fig. 1-2). This research also demonstrated alternative pathways for  $H^+$  and  $H_3O^+$  to move through the altered layer and reach the pristine minerals faster than solid-state diffusion. The presence of this clear boundary between the altered layer and the pristine mineral and the  $H^+$  and  $H_3O^+$  pathways contradict the leached layer theory. Although these observations and their implications on the understanding of dissolution mechanisms of silicate minerals are transforming our perception of mineral and fluid interactions radically (Altree-Williams et al. 2015; Reis, 2015), little work has been conducted on non-silicate minerals, such as apatite.



*Figure 1-2 HRTEM image of the interface between unaltered wollastonite and the surface altered layer, with insert showing EFTEM Si and Ca profiles taken along the A-B transverse. (From Hellmann et al. 2012).*

### 1.3 Chemical Structure and Weathering Behavior of Apatite

The diverse applications of the apatite mineral group are primarily a result of its atomic arrangement and variable composition. Apatite crystallizes as a hexagonal mineral in space group  $P6_3/m$  with a generalized chemical formula of  $Ca_{10}(PO_4)_6(F,Cl,OH)_2$ . Its crystal structure is defined by a framework of  $PO_4$  tetrahedra with two Ca sites and an anion column along the edges of the unit cell. Because of cation and anion substitutions that can occur in its structure there are over 40 known species of apatite, attesting to the robustness of the structure and chemical composition of the mineral group (Hughes and Rakovan, 2015). Additionally, apatite is one of the few minerals that forms an anion solid-solution (Hughes and Rakovan, 2015), which plays a role in its stability under acidic conditions (Adcock et al. 2013; Zhu et al. 2009).

Very little research has been undertaken on molecular-scale weathering processes in phosphate minerals. Apatite dissolution is known to occur under acidic conditions, and the rate at which dissolution occurs is pH dependent (Chairat et al. 2007a, 2007b; Guidry and Mackenzie 2003). It has been suggested that the formation of a leached layer on apatite would occur by apparent preferential leaching of Ca and the formation of a P-enriched,  $CaHPO_4$  leached layer (Chairat et al. 2007a). SEM analysis has shown etch pits on weathered apatite implying dissolution is not a homogenous process over the surface of the mineral (Chairat et al. 2007b; Harouiya et al. 2007).

While most of these studies aimed at defining the controls on phosphorus availability in aqueous systems, the scales of observations remained “coarse,” with observations performed at the macro- to microscale. Due to the limited research on nanoscale dissolution mechanisms of phosphate minerals and the societal need to better

understand apatite dissolution, it is necessary to evaluate the dissolution of apatite at the highest analytical resolution.

#### **1.4 Implications of a Nanoscale CIDR mechanism in Apatite**

Apatite illustrates the quintessential role minerals have played in the evolution of modern society and underscores the importance of research in the mineral sciences (Hughes, 2015). Determining the nanoscale processes responsible for phosphate mineral dissolution has the potential to be transformative for many fields of science including paleo-environment reconstruction, thermochronology, environmental remediation, and treatment of bones and teeth.

Analysis of the isotopic composition of biogenic apatite helps infer past climates, however partial dissolution-reprecipitation of bones at the atomic scale could modify the fractionation of oxygen isotopes (Aufort, 2017). Regarding the use of apatite in thermochronology analysis, a key question to address is to determine how recrystallization and new growth processes influence the ability of apatite to accurately record thermally-activate diffusion profiles (Kirkland et al. 2018). Apatite is also used in environmental remediation for Phosphate Induced Metal Stabilization (PIMS) and radionuclide sequestration (Ewing et al. 2002; Rakovan and Pasteris 2015). Knowledge of apatite precipitation and dissolution mechanisms is crucial for determining safe and sustainable remediation practices (Guan et al. 2018). Anion exchange of F for OH in the apatite material of human tooth enamel, which decreases dental caries, is thought to occur *via* a dissolution and reprecipitation mechanism (Gregory et al. 1991). In 1999, the addition of fluoride to drinking water to prevent dental caries was named one of the

greatest public health achievements of the 20<sup>th</sup> century by the American Center for Disease Control.

The objectives of this study are to (1) determine the nanoscale dissolution mechanism driving apatite weathering (2) determine if the rate and expression of apatite dissolution is a function of its chemical composition and crystal structure. We hypothesize (1) that nanoscale weathering mechanisms of apatite can be investigated using a coherent set of nano- to macro-scale tools and (2) apatite composition and structure affects its weathering behavior. Chapter 2 addresses compositional and structural differences between apatite specimens and their effect on weathering behavior using single crystal XRD. Chapter 3 provides a multiscale investigation of apatite weathering with an emphasis on the nanoscale dissolution mechanism driving apatite dissolution. Finally, Chapter 4 provides a comprehensive conclusion for both chapters.

## 1.5 References Cited

- Adcock, C. T., E. M. Hausrath and P. M. Forster (2013). "Readily available phosphate from minerals in early aqueous environments on Mars." *Nature Geoscience* 6(10): 824-827.
- Altree-Williams, A., Pring, A., Ngothai, Y. and Brugger, J. (2015) Textural and compositional complexities resulting from coupled dissolution–reprecipitation reactions in geomaterials. *Earth-Science Reviews* 150, 628-651.
- Aufort, J., Ségalen, L., Gervais, C., Paulatto, L., Blanchard, M., & Balan, E. (2017). Site specific equilibrium isotopic fractionation of oxygen, carbon and calcium in apatite. *Geochimica et Cosmochimica Acta*, 219, 57-73.
- Banfield, J.F., Jones, B.F. and Veblen, D.R. (1991) An AFM-TEM Study of Weathering and Diagenesis, Abert Lake, Oregon .1. Weathering Reactions in The Volcanics. *Geochimica Et Cosmochimica Acta* 55, 2781-2793.
- Cappelli, C., Lamarca-Irisarri, D., Camas, J., Huertas, F.J. and Van Driessche, A.E.S. (2015) In situ observation of biotite (001) surface dissolution at pH 1 and 9.5 by advanced optical microscopy. *Beilstein Journal of Nanotechnology* 6, 665-673.
- Casey W. H., Westrich H. R., Banfield J. F., Ferruzzi G. and Arnold G. W. (1993) Leaching and reconstruction at the surfaces of dissolving chain-silicate minerals. *Nature* 366, 253–256.
- Casey, W.H., Westrich, H.R. and Arnold, G.W. (1988) Surface-Chemistry of Labradorite Feldspar Reacted with Aqueous-Solutions at pH =2,3, and 12. *Geochimica Et Cosmochimica Acta* 52, 2795-2807.
- Chadwick, O. A., Derry, L. A., Vitousek, P. M., Huebert, B. J., and Hedin, L. O., (1999). Changing sources of nutrients during four million years of ecosystem development: *Nature* (London), v. 397, no. 6719, p. 491-497.
- Chairat, C., Oelkers, E.H., Schott, J. and Lartigue, J.E. (2007a) Fluorapatite surface composition in aqueoussolution deduced from potentiometric, electrokinetic, and solubility measurements, and spectroscopic observations. *Geochimica Et Cosmochimica Acta* 71, 5888-5900.
- Chairat, C., Schott, J., Oelkers, E.H., Lartigue, J.E. and Harouiya, N. (2007b) Kinetics and mechanism of natural fluorapatite dissolution at 25 degrees C and pH from 3 to 12. *Geochimica Et Cosmochimica Acta* 71, 5901-5912.
- Cordell, D., Drangert, J.-O. and White, S. (2009) The story of phosphorus: Global food security and food for thought. *Global Environmental Change* 19, 292-305.

- Daval, D., Bernard, S., Rémusat, L., Wild, B., Guyot, F., Micha, J.S., Rieutord, F., Magnin, V., Fernandez-Martinez, A., (2017). Dynamics of surface altered layer formation on dissolving silicates. *Geochim. Cosmochim. Acta*209, 51–69.
- Daval, D., Hellmann, R., Saldi, G.D., Wirth, R., Knauss, K.G., (2013). Linking nm-scale measurements of the anisotropy of silicate surface reactivity to macroscopic dissolution rate laws: new insights based on diopside. *Geochim. Cosmochim. Acta*107, 121–134.
- Daval, D., Sissmann, O., Menguy, N., Saldi, G.D., Guyot, F., Martinez, I., Corvisier, J., Garcia, B., Machouk, I., Knauss, K.G., Hellmann, R., (2011). Influence of amorphous silica layer formation on the dissolution rate of olivine at 90 degrees C and elevated pCO<sub>2</sub>. *Chem. Geol.*284, 193–209.
- Drouet, C. (2015). A comprehensive guide to experimental and predicted thermodynamic properties of phosphate apatite minerals in view of applicative purposes. *The Journal of Chemical Thermodynamics*, 81, 143-159.
- Ehrlich, H., Hanke, T., Born, R., Fischer, C., Frolov, A., Langrock, T., Worch, H. (2009). Mineralization of biomimetically carboxymethylated collagen fibrils in a model dual membrane diffusion system. *Journal of Membrane Science*, 326(2), 254-259.
- Ewing, R.C., and Wang, L. (2002) Phosphates as nuclear waste forms. *Reviews in Mineralogy and Geochemistry*, 48, 673–700.
- Filippelli, G. M., 2002, The Global Phosphorus Cycle: Reviews in Mineralogy and Geochemistry, v. 48, no. 1, p. 391-425.
- Filippelli, G.M. (2008) The global phosphorus cycle: Past, present, and future. *Elements* 4, 89-95.
- Geisler, T., Nagel, T., Kilburn, M. R., Janssen, A., Icenhower, J. P., Fonseca, R. O. C., Nemchin, A. A. (2015). The mechanism of borosilicate glass corrosion revisited. *Geochimica et Cosmochimica Acta*, 158, 112-129.
- Geisler T., Janssen A., Scheiter D., Stephan T., Berndt J. and Putnis A. (2010) Aqueous corrosion of borosilicate glass under acidic conditions: a new corrosion mechanism. *J. Non-Cryst. Solids* 356, 1458–1465.
- Gordon, L. M., Cohen, M. J., MacRenaris, K. W., Pasteris, J. D., Seda, T., & Joester, D. (2015) Amorphous intergranular phases control the properties of rodent tooth enamel. *Science*, 347(6223), 746. doi:10.1126/science.1258950
- Grant, T.B., Milke, R., Wunder, B., Wirth, R. and Rhede, D. (2014) Experimental study of phlogopite reaction rim formation on olivine in phonolite melts: Kinetics, reaction rates, and residence times. *American Mineralogist* 99, 2211-2226

- Gregory, T. M., Chow, L. C., & Carey, C. M. (1991) A Mathematical Model for Dental Caries: A Coupled Dissolution-Diffusion Process. *Journal of research of the National Institute of Standards and Technology*, 96(5), 593–604.
- Guan, D.-X., Ren, C., Wang, J., Zhu, Y., Zhu, Z., & Li, W., (2018) Characterization of Lead Uptake by Nano-Sized Hydroxyapatite: A Molecular Scale Perspective. *ACS Earth and Space Chemistry*, 2(6), 599-607.
- Guidry, M.W. and Mackenzie, F.T. (2003) Experimental study of igneous and sedimentary apatite dissolution: Control of pH, distance from equilibrium, and temperature on dissolution rates. *Geochimica Et Cosmochimica Acta* 67, 2949-2963.
- Harouiya, N., Chaïrat, C., Köhler, S. J., Gout, R., & Oelkers, E. H. (2007). The dissolution kinetics and apparent solubility of natural apatite in closed reactors at temperatures from 5 to 50 °C and pH from 1 to 6. *Chemical Geology*, 244(3-4), 554-568.
- Hellmann, R., Cotte, S., Cadel, E., Malladi, S., Karlsson, L.S., Lozano-Perez, S., Cabie, M. and Seyeux, A. (2015) Nanometre-scale evidence for interfacial dissolution-reprecipitation control of silicate glass corrosion. *Nature Materials* 14, 307-311.
- Hellmann, R., Wirth, R., Daval, D., Barnes, J.P., Penisson, J.M., Tisserand, D., Epicier, T., Florin, B. and Hervig, R.L. (2012) Unifying natural and laboratory chemical weathering with interfacial dissolution-reprecipitation: A study based on the nanometer-scale chemistry of fluid silicate interfaces. *Chemical Geology* 294, 203-216.
- Hellmann, R., Penisson, J.M., Hervig, R.L., Thomassin, J.H. and Abrioux, M.F. (2003) An EFTEM/HRTEM high-resolution study of the near surface of labradorite feldspar altered at acid pH: evidence for interfacial dissolution-reprecipitation. *Physics and Chemistry of Minerals* 30,192-197.
- Hellmann, R. (1994) The Albite-Water System .1. The Kinetics of dissolution as a Function of pH at 100-Degrees-C, 200-Degrees-C, 300-Degrees-C. *Geochimica Et Cosmochimica Acta* 58, 595-611.
- Hellmann, R. (1995) The Albite-Water System .2. The Time-Evolution of The Stoichiometry of Dissolution as a Function of pH at 100-Degrees-C, 200-Degrees-C, 300-Degrees-C. *Geochimica Et Cosmochimica Acta* 59, 1669-1697.
- Hughes, J.M. and Rakovan, J.F. (2015) Structurally Robust, Chemically Diverse: Apatite and Apatite Supergroup Minerals. *Elements* 11, 165-170.
- Kirkland, C. L., Yakymchuk, C., Szilas, K., Evans, N., Hollis, J., McDonald, B., & Gardiner, N. J. (2018). Apatite: a U-Pb thermochronometer or geochronometer? *Lithos*, 318-319, 143-157.

- La Fontaine, A., Zavgorodniy, A., Liu, H., Zheng, R., Swain, M., & Cairney, J. (2016). Atomic-scale compositional mapping reveals Mg-rich amorphous calcium phosphate in human dental enamel. *Science Advances*, 2(9), e1601145.
- Lee M. R., Hodson M. E., and Parsons I. (1998) The role of intragranular microtexture and microstructures in chemical and mechanical weathering: Direct comparisons of experimentally and naturally weathered alkali feldspars. *Geochim. Cosmochim. Acta* **62**, 2771–2788.
- Maher, K., Steefel, C.I., DePaolo, D.J. and Viani, B.E. (2006) The mineral dissolution rate conundrum: Insights from reactive transport modeling of U isotopes and pore fluid chemistry in marine sediments. *Geochimica Et Cosmochimica Acta* 70, 337-363.
- Michel, F. M., J. D. Rimstidt and K. Kletetschka (2018). 3D printed mixed flow reactor for geochemical rate measurements. *Applied Geochemistry* 89: 86-91.
- Muir, I.J., Bancroft, G.M. and Nesbitt, H.W. (1989) Characteristics of Altered Labradorite Surfaces by SIM and XPS. *Geochimica Et Cosmochimica Acta* 53, 1235-1241.
- Nejad, Z.D., Jung, M. C., and Kim, K.-H. (2018). Remediation of soils contaminated with heavy metals with an emphasis on immobilization technology. *Environmental Geochemistry and Health*, 40(3), 927-953.
- Noiriell, C., Steefel, C.I., Yang, L. and Ajo-Franklin, J. (2012) Upscaling calcium carbonate precipitation rates from pore to continuum scale. *Chemical Geology* 318, 60-74.
- Oelkers, E.H. and Valsami-Jones, E (2008). Phosphate Mineral Reactivity and Global Sustainability. *Elements* 4(2): 83-87.
- O'Neil, J.R. and Taylor, H.P.J. (1967) The oxygen isotope and cation exchange chemistry of feldspars. *American Mineralogist* 52, 1414-1437.
- Parsons, I., Lee, M. R., & Smith, J. V. (1998). Biochemical evolution II: Origin of life in tubular microstructures on weathered feldspar surfaces. *Proceedings of the National Academy of Sciences*, 95(26), 15173
- Pasek, M. A., and Kee, T. P., (2011) On the Origin of Phosphorylated Biomolecules, *Origins of Life: The Primal Self-Organization*, Springer, p. 57-84.
- Petit, J.C., Dran, J.C., Paccagnella, A. and Dellamea, G. (1989) Structural Dependence of Crystalline Silicate Hydration During Aqueous Dissolution. *Earth and Planetary Science Letters* 93, 292-298.

- Powner, M. W., Gerland, B., and Sutherland, J. D., 2009, Synthesis of activated pyrimidine ribonucleotides in prebiotically plausible conditions: *Nature*, v. 459, no. 7244, p. 239-242
- Putnis A (2002) Mineral replacement reactions: from macroscopic observations to microscopic mechanisms *Mineral Mag* 66:689–708
- Putnis, A., & Putnis, C. V. (2007). The mechanism of reequilibration of solids in the presence of a fluid phase. *Journal of Solid-State Chemistry*, 180(5), 1783-1786.
- Putnis, A. (2016) Control of silicate weathering by interface-coupled dissolution-precipitation processes at the mineral-solution interface. *Geology* 44, 567-570.
- Putnis, A. (2015) Sharpened interface. *Nature Materials* 14, 261-262.
- Putnis, A. (2014) Why Mineral Interfaces Matter. *Science* 343, 1441-1442.
- Putnis, C.V. and Ruiz-Agudo, E. (2013) The Mineral-Water Interface: Where Minerals React with the Environment. *Elements* 9, 177-182.
- Rakovan, J. (2002). "Growth and Surface Properties of Apatite." *Reviews in Mineralogy and Geochemistry* 48(1): 51-86.
- Reis, F.D.A.A. (2015) Modeling the growth of an altered layer in mineral weathering. *Geochimica Et Cosmochimica Acta* 166, 298-311.
- Rigali, Mark J., Brady, Patrick V., & Moore, Robert C.. *Radionuclide removal by apatite*. United States. doi:10.2138/am-2016-5769.
- Ruiz-Agudo, E., King, H.E., Patino-Lopez, L.D., Putnis, C.V., Geisler, T., Rodriguez-Navarro, C. and Putnis, A. (2016) Control of silicate weathering by interface-coupled dissolution precipitation processes at the mineral-solution interface. *Geology* 44, 567-570.
- Ruiz-Agudo, E., Putnis, C.V. and Putnis, A. (2014) Coupled dissolution and precipitation at mineral-fluid interfaces. *Chemical Geology* 383, 132-146.
- Ruiz-Agudo, E., Putnis, C.V., Rodriguez-Navarro, C., Putnis, A., 2012. Mechanism of leached layer formation during chemical weathering of silicate minerals. *Geology* 40, 947–950. Saldi, G.D., Daval, D., Guo, H., Guyot, F., Bernard, S., Le Guillou, C., Davis, J.A., Knauss, K.G., (2015) Mineralogical evolution of Fe–Si-rich layers at the olivine–water interface during carbonation reactions. *Am. Mineral.* 100, 2655–2669.
- Schaad Ph., Poumier F., Voegel J. C., and Gramain Ph. (1997) Analysis of calcium hydroxyapatite dissolution in non-stoichiometric solutions. *Coll. Surf. A: Physicochem. Eng. Asp.* **121**, 217–228.

- Schwartz, A. W., (2006) Phosphorus in Prebiotic Chemistry: Philosophical Transactions: Biological Sciences, v. 361, no. 1474, p. 1743-1749.
- Schweda, P., Sjoberg, L. and Sodervall, U. (1997) Near-surface composition of acid-leached labradorite investigated by SIMS. *Geochimica Et Cosmochimica Acta* 61, 1985-1994.
- Steeffel, C.I., Appelo, C.A.J., Arora, B., Jacques, D., Kalbacher, T., Kolditz, O., Lagneau, V., Lichtner, P.C., Mayer, K.U., Meeussen, J.C.L., Molins, S., Moulton, D., Shao, H., Simunek, J., Spycher, N., Yabusaki, S.B. and Yeh, G.T. (2015a) Reactive transport codes for subsurface environmental simulation. *Computational Geosciences* 19, 445-478.
- Steeffel, C.I., DePaolo, D.J. and Lichtner, P.C. (2005) Reactive transport modeling: An essential tool and a new research approach for the Earth sciences. *Earth and Planetary Science Letters* 240, 539-558.
- Valsami-Jones, E., Ragnarsdottir, K.V., Putnis, A., Bosbach, D., Kemp, A.J. and Cressey, G. (1998) The dissolution of apatite in the presence of aqueous metal cations at pH 2-7. *Chemical Geology* 151, 215-233.
- Wang, Y., Zhang, L., Hu, M., Liu, H., Wen, W., Xiao, H., & Niu, Y. (2008). Synthesis and characterization of collagen-chitosan-hydroxyapatite artificial bone matrix. *86A(1)*, 244-252.
- White, A.F. and Brantley, S.L. (2003) The effect of time on the weathering of silicate minerals: why do weathering rates differ in the laboratory and field? *Chemical Geology* 202, 479- 506.
- Zhu, Y., Zhang X., Chen Y., Xie Q., Lan J., Qian M., He N., (2009). "A comparative study on the dissolution and solubility of hydroxylapatite and fluorapatite at 25°C and 45°C." *Chemical Geology* 268(1): 89-96.

## **Chapter 2: Chemical and Structural Characterization of Apatite: The Role of Anions and Implication for Weathering Behavior**

### **2.1 Introduction**

Although apatite minerals are not considered rock forming minerals, they occur as accessory minerals in every geologic setting on Earth and as one of the most common biominerals, composing the bones, teeth, and exoskeletons of some animals. It is also the most abundant phosphate mineral, and its dissolution is the primary source of phosphorus (P) in the environment (Filippelli, 2008). Moreover, its weathering reactions played a crucial role in the development of life as phosphorus is the backbone of our DNA (Adcock et al. 2013; Cordell et al. 2009). Due to apatite's ubiquity and importance in sustaining life, its characteristics and behavior are of consequence to many fields including, geology, agronomy, environmental remediation, medicine and dentistry (Hughes and Rakovan 2015).

Apatite is amongst the most efficient contaminant scavengers in soils and waters (Nejad et al. 2018; Rigali et al. 2016). Knowledge of apatite stability, precipitation and dissolution mechanisms is paramount in the development of sustainable remediation (Guan et al. 2018). Analysis of the isotopic composition of biogenic apatite helps infer past climates (Aufort et al. 2017). Calcium phosphate mineralization and dissolution are of interest for bone and dental decalcification and potential repair (Wang et al. 2008; Ehrlich et al. 2010; Gordon et al. 2015, La Fontaine et al. 2016). Coating prostheses with apatite prior to insertion has been shown to improve bone-prosthesis melding and healing rates (Constantz and Osaka 1994).

The diverse applications of the apatite mineral group are primarily a result of its atomic arrangement and variable composition. Apatite is a hexagonal mineral

crystallizing in space group  $P6_3/m$  with a generalized chemical formula of  $\text{Ca}_{10}(\text{PO}_4)_6(\text{F},\text{Cl},\text{OH})_2$ . Its crystal structure is defined by a framework of  $\text{PO}_4$  tetrahedra with two Ca sites (Ca1 and Ca2) and an anion column along the  $c$ -axis on the corners of the unit cell (Fig. 2-1). The anion column is bonded to three Ca2 atoms that form a triangle on a mirror plane at  $z = \frac{1}{4}$  and  $\frac{3}{4}$ . Of particular interest, apatite is one of the few minerals that forms an anion solid solution (Hughes and Rakovan 2015). In pure endmember fluorapatite, fluorine atoms occupy the anion column on the mirror plane. In pure endmember hydroxylapatite and chlorapatite, hydroxyl and chlorine atoms occupy the anion column either above or below the mirror plane in order to maintain  $P6_3/m$  symmetry (Hughes et al. 2014).

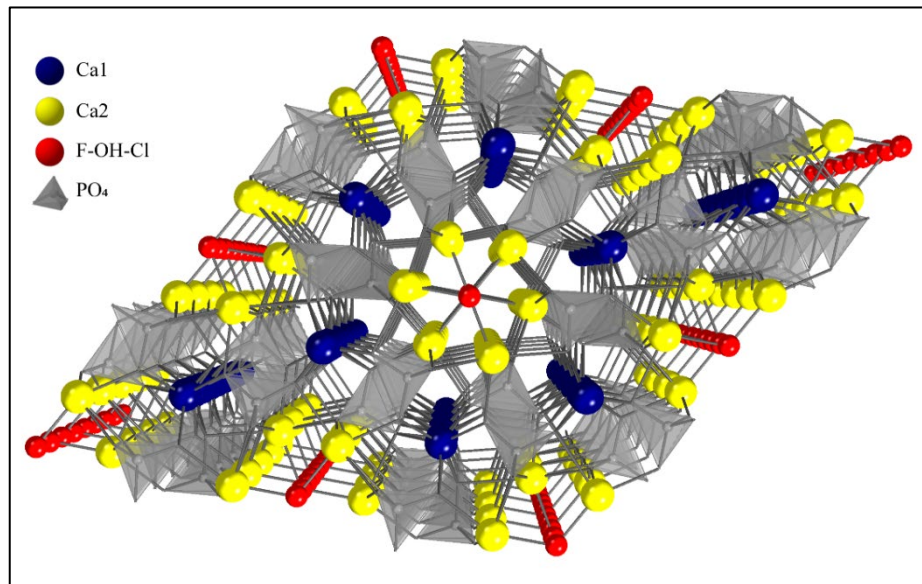


*Figure 2-1. Crystal structure of apatite looking down the C axis.*

Due to steric constraints however, solid-solution cannot occur with F, Cl, OH in their pure endmember atomic positions (Hughes et al. 1990). These steric constraints cause the positions of the anions to vary along the  $c$ -axis based on the apatite's endmember composition. The resulting anion positions are determined by several factors summarized in Hughes et al. (2016), such as anion size, electrostatic repulsion due to the

nearest neighbor in the anion column, dissymmetry in the structure, and electrostatic attraction caused by the surrounding Ca<sub>2</sub> atoms. These constraints lead to a flexible structure allowing apatite to accommodate F, Cl, and OH anions, which significantly vary in size (F<sup>-</sup> = 1.26 Å, OH<sup>-</sup> = 1.33 Å, Cl<sup>-</sup> = 1.72 Å; Jenkins and Thakur 1979; Kelly et al. 2017).

Pure endmember apatites vary significantly in stability based on the experimentally determined Gibbs free energy of formation ( $\Delta G_f^\circ$ ), with fluorapatite being the strongest and chlorapatite the weakest (Drouet et al. 2015). The  $\Delta G_f^\circ$  for fluorapatite and the chlorapatite are -12838 and -12506.5 kJ mol<sup>-1</sup> respectively. Because the stability of apatite depends so heavily on endmember composition, studying the structural arrangement of the anion column is fundamental to improving our understanding of apatite dissolution. The objective of this study was to characterize the chemical composition and structure of two types of naturally occurring apatite, Durango fluorapatite and hydroxyl-chlorapatite. Characterization of these apatites was conducted as part of a larger study on how the chemical and structural differences in the apatites affect weathering behavior.

## **2.2 Materials and Methods**

### **2.2.1 Apatite specimens**

Euhedral crystals of yellow fluorapatite from Durango, Mexico and dark blue hydroxyl-chlorapatite from an unknown location were acquired from online vendors. The prismatic fluorapatite and hydroxyl-chlorapatite samples presented well-developed {001}, {101}, and {101} faces, approximately 1 to 4 cm in length and less than 1 cm in width (Fig. 2-2).



Figure 2-1. Euhedral crystals of a) Durango fluorapatite and b) hydroxyl-chlorapatite.

### 2.2.2 Single-Crystal XRD

Two samples of hydroxyl-chlorapatite and two samples of fluorapatite (Durango) were analyzed by single-crystal XRD using methods adapted from Hughes et al. (2018). Apatite samples were ground into 80  $\mu\text{m}$  spheres and X-ray diffraction data was collected with a Bruker Apex II CCD single-crystal diffractometer using graphite-monochromated  $\text{MoK}\alpha$  radiation. For both samples, redundant data were collected for a sphere of reciprocal space (4500 frames,  $0.20^\circ$  scan width; average redundancy  $\approx 16$ ) and were integrated and corrected for Lorentz and polarization factors and absorption using the Bruker Apex2 package of programs. The atomic arrangement was refined in space group  $P6_3/m$ , on  $F^2$ , with SHELXL-97 (Sheldrick 2008), using neutral atom scattering factors and full-matrix least-squares, minimizing the function  $\sum w(F_{\text{obs}}^2 - F_{\text{calc}}^2)^2$  where  $F_{\text{obs}}$  is the observed structure factor and  $F_{\text{calc}}$  is the calculated structure factor, with no restraints. All atoms were refined with anisotropic temperature factors except the column anions; an extinction coefficient was also refined. As noted in Hughes et al. (2016) the use of anisotropic atomic displacement factors for the column anions yields unreasonable values of  $U_{33}$ , an anisotropy that masks the positions of anion sites occupied by small fractions of a column anion. The occupancy values of the column anions were not constrained.

During the structure refinement all sites but the anion column sites were assumed to be fully occupied, an assumption supported by testing release of occupancy factors; the

superior final  $R_1$  values ( $0.0144 \leq R_1 \leq 0.0165$ ) in the final structure refinements also corroborated that assumption.  $R_1$  value describes the final and overall quality of the structural refinement, where  $R_1 = \frac{\sum |F_{obs} - F_{calc}|}{\sum |F_{obs}|}$  with  $F_{obs}$  the observed structure factor and  $F_{calc}$  the calculated structure factor.

### 2.2.3 Bond Valence Calculations

Bond valence was calculated for each anion in the anion column, where the valence of an atom is equal to the sum of each bond it forms. Ideally the valence of an atom is 1, an atom with a valence below 1 being underbonded and an atom with a bond valence above 1 being overbonded. Bond valence is a function of bond length with the bond valence for an individual bond defined by the equation  $v_i = \exp\left(\frac{R_o - R_i}{b}\right)$ , where  $v_i$  is the bond valence,  $R_o$  is the ideal bond length when the element  $i$  has an exact valence of 1,  $R_i$  is the observed bond length, and  $b$  is an empirical constant typically defined as 0.37 Å. Furthermore, the valence of an atom is defined by the sum of its surrounding individual bond valences where  $V = \sum(v_i)$ .

## 2.3 Results & Discussion

The experimentally determined sum of column anions, determined without constraints or restraints, yielded a range between 2.09 and 2.13 atoms per formula unit (apfu). The slight deviation from the ideal value of 2.00 apfu (5–7%) may result from the use of neutral-atom scattering factors rather than partially or fully ionized scattering factors. We believe these analyses obtained by site-occupancy refinement are at least as accurate and precise as electron microprobe measurements of F and the calculation of O(H) by the difference (Hawthorne and Grice 1990; Stormer et al. 1993; Stock et al. 2015; Kelly et al. 2017).

### 2.3.1 Fluorapatite

The structures of two samples of Durango fluorapatite were both solved and refined to  $R_1$  values of 0.0151 and 0.0165 using single crystal XRD. The crystal chemistry of the fluorapatite samples was in agreement with formula of  $\text{Ca}_{10}(\text{PO}_4)_6(\text{F}_{1.30}\text{OH}_{0.78})_{\Sigma 2.08}$ , and  $\text{Ca}_{10}(\text{PO}_4)_6(\text{F}_{1.41}\text{OH}_{0.71})_{\Sigma 2.12}$ . Table 2-1 shows the atomic coordinates and equivalent isotropic atomic displacement parameters for a representative sample of fluorapatite. The anion column of Durango fluorapatite is composed of approximately two thirds F and one third OH. The arrangement of this anion column is acceptable for Durango fluorapatite and similar to an OH-rich fluorapatite described in Chairat et al. (2007a, 2007b).

Two column anion sites were refined in the Durango fluorapatite. Table 2-2 lists the z coordinates of the column anions and the portion of each site that is occupied. A F site was found at special position (0,0,1/4) on the mirror plane, as is in endmember fluorapatite. An OH site was found at  $z = 0.193$  occurring above or below the mirror plane, close to anion column sites in endmember hydroxylapatite. Figure 2-3 depicts the reversal of the Durango fluorapatite anion column to maintain a mirror plane at  $z = 1/4$  and remain in space group  $P6_3/m$ .

Table 2-1. Atomic coordinates and equivalent isotropic atomic displacement parameters ( $\text{\AA}^2$ ) for fluorapatite

| Atom | $x/a$                    | $y/b$       | $z/c$       | $U_{eq}^1$  |
|------|--------------------------|-------------|-------------|-------------|
| Ca1  | 2/3                      | 1/3         | 0.01008(4)  | 0.01195(8)  |
| Ca2  | 0.76054(16) <sup>2</sup> | 0.75350(17) | 1/4         | 0.0082(10)  |
| P    | 0.36899(4)               | 0.39846(4)  | 1/4         | 0.00701(7)  |
| O1   | 0.48456(12)              | 0.32696(13) | 1/4         | 0.01191(17) |
| O2   | 0.46647(12)              | 0.58793(12) | 1/4         | 0.01404(18) |
| O3   | 0.65819(10)              | 0.91545(9)  | 0.07038(11) | 0.01621(14) |
| F    | 0                        | 0           | 1/4         | 0.0105(9)   |
| OH   | 0                        | 0           | 0.193(2)    | 0.011(2)    |

<sup>1</sup> $U_{eq}$  is defined as one third of the trace of the orthogonal  $U_{ij}$  tensor. <sup>2</sup>Error in concised form

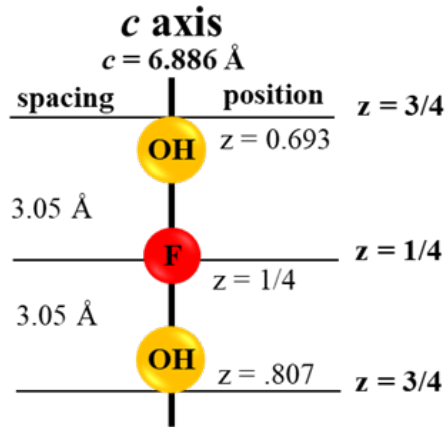


Figure 2-2. Depiction of the anion column reversal, necessary to maintain symmetry and remain in space group  $P6_3/m$ , with an acceptable sequence of atoms in Durango fluorapatite.

Table 2-2. Value of  $z$  for column anions in  $(0,0,z)$  sites and percentage of total column anion occupancy in Both Durango apatite samples

| F   | Site % | OH    | Site % | Anion Column Occ.       |
|-----|--------|-------|--------|-------------------------|
| 1/4 | 62.5   | 0.193 | 37.5   | ( $F_{1.30}OH_{0.78}$ ) |
| 1/4 | 66.5   | 0.190 | 33.5   | ( $F_{1.41}OH_{0.71}$ ) |

### 2.3.2 Hydroxyl-chlorapatite

The structures of two samples of hydroxyl-chlorapatite were both solved for and refined to a  $R_1$  value of 0.0144 using single crystal XRD. The crystal chemistry of the hydroxyl-chlorapatite samples were in agreement with respective formulas of  $\text{Ca}_{10}(\text{PO}_4)_6(\text{OH}_{1.92}\text{Cl}_{0.18})_{\Sigma 2.10}$  and  $\text{Ca}_{10}(\text{PO}_4)_6(\text{OH}_{1.96}\text{Cl}_{0.17})_{\Sigma 2.13}$ . Table 2-3 lists the atomic coordinates and equivalent isotropic atomic displacement parameters for a representative sample of hydroxyl-chlorapatite. No F was accommodated in the hydroxyl-chlorapatite structure at  $(0, 0, \frac{1}{4})$ . Four anion column sites previously observed by Hughes et al. (2016) were found in the hydroxyl-chlorapatite. Table 2-4 lists the z coordinates of the column anions and the portion of each site that is occupied. An OH site was found at  $z = 0.226$  with an atomic distance of 2.319 Å from Ca2.

A unique site was found at  $z = 0.176$  that accommodates either OH or Cl. This unique site was only identified recently in synthetic and natural apatites by Hughes et al. (2016) and Kelly et al. (2017). A Cl anion is unduly large to occupy the same atomic position as an OH anion without disordering the Ca2 sites. Therefore, for OH and Cl anions to occupy the ClOH site and maintain sufficient bond distances from the neighboring Ca2 sites, the Ca2 site breaks into two different sites Ca2 and Ca2'. The Ca2 sites bonds to the ClOH site and accommodates OH at an atomic distance of 2.369 Å, and the Ca2' sites bonds to the ClOH site and accommodates Cl at distance of 2.662 Å (Fig. 2-4). These atomic distances are similar to 2.45 Å and 2.72 Å, respectively reported in Hughes et al. (2016). The bond distances observed for each respective anion are close to ideal for OH and Cl to Ca bonds. OH, or Cl can occupy the ClOH site, however, the ClOH site in this hydroxyl-chlorapatite is primarily occupied by Cl (Table 2-4).

Table 2-3. Atomic coordinates and equivalent isotropic atomic displacement parameters ( $\text{\AA}^2$ ) for hydroxyl-chlorapatite

| Atom            | $x/a$                  | $y/b$       | $z/c$       | $U_{eq}^1$     |
|-----------------|------------------------|-------------|-------------|----------------|
| Ca1             | 2/3                    | 1/3         | 0.00129(4)  | 0.01195(8)     |
| Ca2             | 0.7576(3) <sup>2</sup> | 0.7505(3)   | 1/4         | 0.01035(19)    |
| Ca2'            | 0.730(6)               | 0.715(7)    | 1/4         | 0.01035(19)    |
| P               | 0.36903(4)             | 0.39850(4)  | 1/4         | 0.00789(8)     |
| O1              | 0.48444(12)            | 0.32692(12) | 1/4         | 0.01258(17)    |
| O2              | 0.46613(12)            | 0.58768(12) | 1/4         | 0.01580(19)    |
| O3              | 0.65770(10)            | 0.91509(9)  | 0.07056(11) | 0.01861(15)    |
| OH              | 0                      | 0           | 0.226(2)    | 0.0147(8)      |
| ClOH            | 0                      | 0           | 0.176(8)    | 0.027(5)       |
| Cl <sub>a</sub> | 0                      | 0           | 0           | 0.02(2)        |
| Cl <sub>b</sub> | 0                      | 0           | 0.086       | Not calculated |

<sup>1</sup> $U_{eq}$  is defined as one third of the trace of the orthogonal  $U_{ij}$  tensor.

<sup>2</sup>Error in concised form

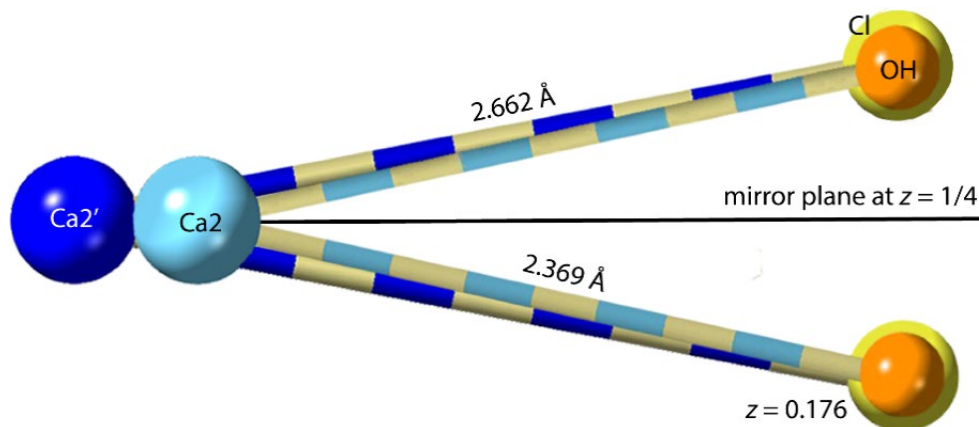


Figure 2-4. Disordering of Ca2 to Ca2' to accommodate the ClOH site to accommodate Cl.

Table 2-4. Value of  $z$  for column anions in  $(0,0,z)$  sites and percentage of total column anion occupancy in both natural hydroxyl-chlorapatite samples

| OH    | Site % | ClOH <sup>1</sup> | Site % | Cl <sub>a</sub> | Site % | Cl <sub>b</sub> | Site % <sup>2</sup> | Anion Column Occ.                        |
|-------|--------|-------------------|--------|-----------------|--------|-----------------|---------------------|--|
| 0.226 | 91.3   | 0.176             | 8.0    | 0               | 0.7    | 0.086           | ~                   | (OH <sub>1.92</sub> Cl <sub>0.18</sub> ) |
| 0.226 | 92.1   | 0.173             | 7.1    | 0               | 0.8    | 0.084           | ~                   | (OH <sub>1.96</sub> Cl <sub>0.17</sub> ) |

<sup>1</sup> ClOH site: ~2 % OH and ~98 % Cl

<sup>2</sup> The Cl<sub>b</sub> makes up a negligible portion of the anion column.

An additional Cl<sub>a</sub> site was found at  $z = 0$ , which is known to occur in OH-Cl and F-Cl binary apatites (Hughes et al. 2014, 2016). This site is located halfway between two mirror planes causing the Cl<sub>a</sub> site to bond to six Ca<sub>2</sub> sites, which accounts for the unusually long bond distance of 2.885 Å (Hughes et al. 2016). A third, sparsely occurring, Cl<sub>b</sub> site was found at  $z = 0.086$ , close to the anion column site in endmember chlorapatite. The Cl<sub>b</sub> site exists in the structure based on the difference peaks and is required to reverse the anion column and maintain P6<sub>3</sub>/m symmetry. However, the Cl<sub>b</sub> site makes up a negligible portion of the anion column sites. Although Cl makes up a small portion of the anion column, three of the four anion column sites can accommodate Cl.

Figure 2-5 depicts the reversal of the hydroxyl-chlorapatite anion column to maintain a mirror plane at  $z = \frac{1}{4}$  and remain in space group P6<sub>3</sub>/m. This anion column sequence shows one Cl<sub>a</sub> site at  $z = 0$  and one ClOH site at  $z = 0.176$  occupied by an OH rather than a Cl, which allows for the Cl<sub>a</sub> and ClOH sites to maintain a reasonable distance from their neighboring Cl<sub>b</sub> sites, as explained in Hughes et al. (2016). We suggest that OH is occupying the Cl<sub>a</sub> site through a mechanism proposed by Mackie and Young (1974) for fluor-chlorapatite and observed in both F-Cl and Cl-OH binary apatite by Hughes et al. (2014, 2016). F or in this case OH can occupy the Cl site at (0,0,0) if the position is found in the structural refinement and the interatomic distances between anion column occupants remain a reasonable length apart. Conversely, Cl cannot occupy a F or OH site because the Ca<sub>2</sub>-Cl distances would be too short. This occurrence is further supported by the ordering of atoms required for anion column reversal in the hydroxyl-chlorapatite.

Because apatite forms an anion solid-solution, most naturally occurring apatite do not exist in their pure endmember forms (Hughes and Rakovan 2015). Apatite preferentially crystallizes with F due to the laws of thermodynamics, therefore, for OH-Cl binary apatite to form the source magma or fluid must have been completely depleted in F (Drouet 2015). The naturally occurring hydroxyl-chlorapatites characterized in this study are structurally most similar to synthetic OH-Cl apatites with anion compositions of  $\text{OH} > \text{Cl}$  and  $\text{OH} \approx \text{Cl}$  reported in (Hughes et al. 2016). All anion column sites discussed in this section were previously identified in synthetic OH-Cl binary apatite by Hughes et al. (2016) and naturally occurring zoned F-OH-Cl ternary apatites by Kelly et al. (2017). Compared to previously identified ClOH sites (Hughes et al. 2016; Kelly et al. 2017), the present ClOH sites are primarily occupied by Cl, with a mere 1-2% of the site occupied by OH.

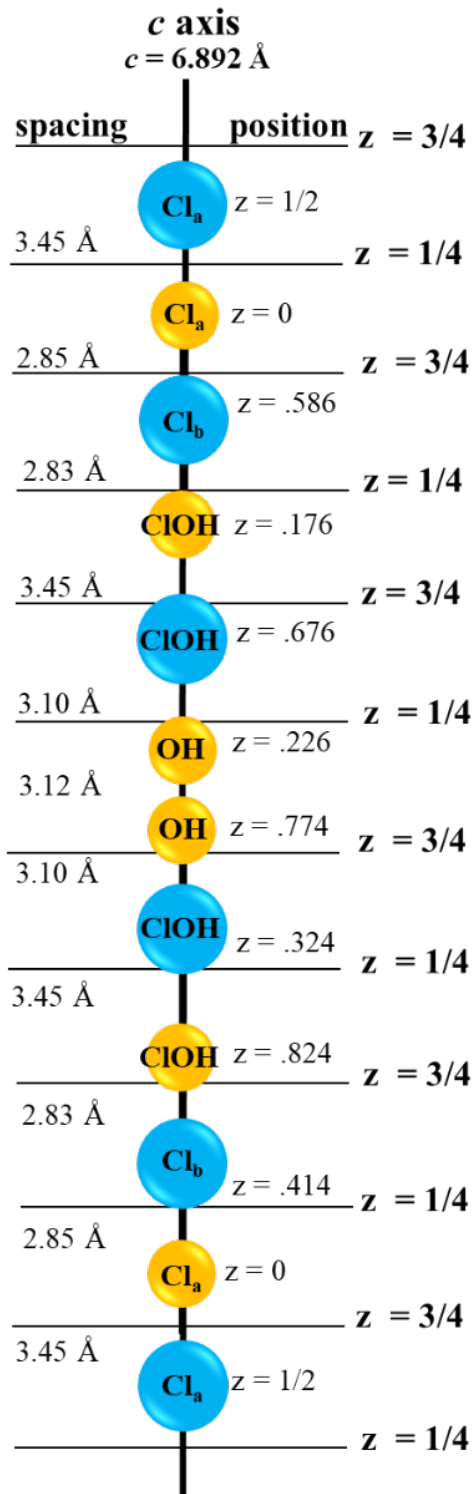


Figure 2-5. Depiction of the anion column reversal, necessary to maintain symmetry and remain in space group  $P6_3/m$ , with an acceptable sequence of atoms in the hydroxyl-chlorapatite.

### 2.3.3 Effect of Anion Column Arrangement on Bond Distances

The anion column arrangement also determines the bond distance or length between Ca<sub>2</sub> and the anion column. Ca<sub>2</sub>-anion bonds vary in length depending on the position of the ion in the anion column and the number of Ca<sub>2</sub> atoms it is bonded to (its coordination number) (Hughes 2015). Increasing the coordination number from three to six for Cl<sub>a</sub> allows for a longer bond length. OH, and Cl ions are larger than F ions leading to a longer bond between Ca<sub>2</sub> atoms and the anion column in hydroxyl-chlorapatite compared to Durango fluorapatite (Table 2-5). The Ca<sub>2</sub>-OH bonds in Durango fluorapatite were significantly shorter compared to the Ca<sub>2</sub>-OH and Ca<sub>2</sub>-ClOH (occupied by OH) bonds in the hydroxyl-chlorapatite. The Ca<sub>2</sub>-Cl<sub>a</sub> and Ca<sub>2</sub>'-Cl<sub>b</sub> bonds were significantly longer but make up a very small percentage of the anion column compared to Ca<sub>2</sub>'-ClOH (occupied by Cl). Additionally, Ca<sub>2</sub>-Cl<sub>a</sub> was bonded to 6 Ca<sub>2</sub> atoms lengthening the Ca<sub>2</sub>-Cl<sub>a</sub> bonds.

### 2.3.4 Implications for Weathering Behavior

There is clearly a compositional control on apatite dissolution in the anion column. According to the American Center for Disease Control the large decline in dental caries in the United States since the 1960s, is attributed to the fluoridation of hydroxylapatite *via* fluoridated tooth paste and public water supplies. Adcock et al. (2013) found that pure endmember chlorapatite dissolves 1.7-8.3 times faster than pure endmember fluorapatite over the same pH range. Although pure endmember apatites do not readily occur in nature, pure endmember compositions likely represent the upper and lower bounds of apatite solubility (Adcock et al. 2013). Therefore, dissolution rates of binary and ternary apatites are expected to fall somewhere in between these pure endmember dissolution rates. Based on the compositional differences in the anion

column, hydroxyl-chlorapatite is expected to have a faster dissolution rate than Durango fluorapatite. Dissolution rates for both apatites characterized in this study may be relatively closer due to compositional overlap of OH in the anion column of Durango fluorapatite and hydroxyl-chlorapatite.

The solubility and dissolution rates of apatite is determined by several factors, anion column composition, atomic size, bond strength, and hydrogen bonding. Ions that constitute the anion column in apatite decrease in atomic size as follows: F > OH > Cl (Jenkins and Thakur 1979). Weaker bonds in the anion column are thought to increase solubility, and thus dissolution rate of apatite (Adcock 2014). Accordingly, bond energies decrease between Ca<sup>2+</sup> and the anion column as follows: Ca-F > Ca-OH > Ca-Cl, where Ca-F = 529 kJ/mol, Ca-OH = 498 kJ/mol, and Ca-Cl = 409 kJ/mol (Luo 2007). Bond strength is a function of bond length (Brese and O'keeffe 1991), however bond length and bond strength are not linear functions (Hughes et al. 2018). The bond valence sum for each anion site, as well as, the bond valence to anion column are shown in Table 2-5. Durango fluorapatite has a bond valence sum to the anion column of 1.03 and chlor-hydroxylapatite has a bond valence sum to the anion column of 1.18. Chlor-hydroxylapatite is therefore dramatically over bonded compared to Durango fluorapatite, by amount that may not allow for a very stable structure (Hughes et al. 2018). The  $\Delta G_f^\circ$  for Durango fluorapatite and the chlor-hydroxylapatite were calculated using an additive model developed by Drouet (2015) to evaluate standard thermodynamic properties of complex apatite compositions. The  $\Delta G_f^\circ$  for Durango fluorapatite and the chlor-hydroxylapatite is  $-12746.5 \pm 5.5$  and  $-12574.5 \pm 0.5$  respectively. Because

Durango fluorapatite forms at a lower  $\Delta G_f^\circ$  than chlor-hydroxylapatite it is expected to be a thermodynamically more stable apatite structure (Drouet 2015).

*Table 2-5. Bond length and bond valence sum between Ca2 atoms and column anion sites*

| Bond                  | Bond Length (Å) | Bond Valence Sum (vu) | Sum to Anion Column (vu) |
|-----------------------|-----------------|-----------------------|--------------------------|
| fluorapatite          |                 |                       |                          |
| Ca2-F                 | 2.273           | 0.936                 | 1.033                    |
| Ca2-OH                | 2.299           | 1.223                 |                          |
| hydroxyl-chlorapatite |                 |                       |                          |
| Ca2-OH                | 2.319           | 1.159                 | 1.175                    |
| Ca2-ClOH (OH)         | 2.369           | 1.012                 |                          |
| Ca2'-ClOH (Cl)        | 2.662           | 1.366                 |                          |
| Ca2-Cl <sub>a</sub>   | 2.885           | 1.492                 |                          |
| Ca2-Cl <sub>b</sub>   | 2.77            | 1.018                 |                          |

## 2.4 Conclusions

Hydroxyl-chlorapatite has larger ions in the anion column corresponding to longer bonds between the anion column sites and Ca2 sites than Durango fluorapatite.

Therefore, hydroxyl-chlorapatite is expected to weather faster than Durango fluorapatite.

Understanding how solid-solution exists in apatite is vital for studying the breakdown of inorganic and organic apatite. Apatite is a ubiquitous mineral existing in almost all know environments and the availability of P through weathering of apatite is a process indispensable to life. Apatite stability has implications for teeth and bone demineralization and remineralization, sustainability of heavy metal and radionuclide sequestration via apatite, and the accuracy of geochronologic apatite records. Because apatite dissolution is primarily controlled by anionic composition, determining apatite solubility and dissolution processes may depend heavily on the mechanisms by which solid-solution exists in the column anion column.

## 2.5 References Cited

- Adcock, C. T., E. M. Hausrath and P. M. Forster (2013). "Readily available phosphate from minerals in early aqueous environments on Mars." *Nature Geoscience* 6(10): 824-827.
- Adcock, Christopher (2014). "Mars-Relevant Phosphate Minerals and Implications for Martian Habitability" UNLV Theses, Dissertations, Professional Papers, and Capstones. 2162.
- Aufort, J., Ségalen, L., Gervais, C., Paulatto, L., Blanchard, M., & Balan, E. (2017). Site specific equilibrium isotopic fractionation of oxygen, carbon and calcium in apatite. *Geochimica et Cosmochimica Acta*, 219, 57-73.
- Brese, N.E., and O’Keeffe, M. (1991) Bond-valence parameters for solids. *Acta Crystallographica*, B47, 192–197.
- Clark, C. M. (2016). Single-crystal Structure Refinement (SREF). Retrieved from [https://serc.carleton.edu/research\\_education/geochemsheets/SREF.html](https://serc.carleton.edu/research_education/geochemsheets/SREF.html)
- Cordell, D., Drangert, J.-O. and White, S. (2009) The story of phosphorus: Global food security and food for thought. *Global Environmental Change* 19, 292-305.
- Drouet, C. (2015). A comprehensive guide to experimental and predicted thermodynamic properties of phosphate apatite minerals in view of applicative purposes. *The Journal of Chemical Thermodynamics*, 81, 143-159.
- Filippelli, G.M. (2008) The global phosphorus cycle: Past, present, and future. *Elements* 4, 89-95.
- Gordon, L. M., Cohen, M. J., MacRenaris, K. W., Pasteris, J. D., Seda, T., & Joester, D. (2015) Amorphous intergranular phases control the properties of rodent tooth enamel. *Science*, 347(6223), 746.
- Gregory, T. M., Chow, L. C., & Carey, C. M. (1991) A Mathematical Model for Dental Caries: A Coupled Dissolution-Diffusion Process. *Journal of research of the National Institute of Standards and Technology*, 96(5), 593–604.
- Guan, D.-X., Ren, C., Wang, J., Zhu, Y., Zhu, Z., & Li, W., (2018) Characterization of Lead Uptake by Nano-Sized Hydroxyapatite: A Molecular Scale Perspective. *ACS Earth and Space Chemistry*, 2(6), 599-607.
- Chairat, C., Oelkers, E.H., Schott, J. and Lartigue, J.E. (2007a) Fluorapatite surface composition in aqueous solution deduced from potentiometric, electrokinetic, and solubility measurements, and spectroscopic observations. *Geochimica Et Cosmochimica Acta* 71, 5888-5900.

- Chairat, C., Schott, J., Oelkers, E.H., Lartigue, J.E. and Harouiya, N. (2007b) Kinetics and mechanism of natural fluorapatite dissolution at 25 degrees C and pH from 3 to 12. *Geochimica Et Cosmochimica Acta* 71, 5901-5912.
- Constantz, B.R., and Osaka, G.C. (1994) Hydroxyapatite prosthesis coatings. U.S. Patent 5,279,831 A.
- Cordell, D., Drangert, J.-O. and White, S. (2009) The story of phosphorus: Global food security and food for thought. *Global Environmental Change* 19, 292-305.
- Ehrlich, H., Hanke, T., Born, R., Fischer, C., Frolov, A., Langrock, T., Worch, H. (2009). Mineralization of biomimetically carboxymethylated collagen fibrils in a model dual membrane diffusion system. *Journal of Membrane Science*, 326(2), 254-259.
- Ewing, R.C., and Wang, L. (2002) Phosphates as nuclear waste forms. *Reviews in Mineralogy and Geochemistry*, 48, 673–700.
- Hawthorne, F.C., and Grice, J.D. (1990) Crystal-structure analysis as a chemical analytical method: application to light elements. *Canadian Mineralogist*, 28, 693–702.
- Hughes, J.M., Cameron, M., and Crowley, K.D. (1990) Crystal structures of natural ternary apatites: solid solution in the  $\text{Ca}_5(\text{PO}_4)_3\text{X}$  (X = F, OH, Cl) system. *American Mineralogist*, 75, 295–304.
- Hughes, J.M., Nekvasil, H., Ustunisik, G., Lindsley, D.H., Coraor, A.E., Vaughn, J., Phillips, B., McCubbin, F.M., and Woerner, W.R. (2014) Solid solution in the fluorapatite-chlorapatite binary system: High-precision crystal structure refinements of synthetic F-Cl apatite. *American Mineralogist*, 99, 369–376.
- Hughes, J.M. (2015) The many facets of apatite. Mineralogical Society of America Presidential Address. *American Mineralogist*, 100, 1033–1039.
- Hughes, J.M. and Rakovan, J.F. (2015) Structurally Robust, Chemically Diverse: Apatite and Apatite Supergroup Minerals. *Elements* 11, 165-170.
- Hughes, J. M., Harlov, D., Kelly, S. R., Rakovan, J., & Wilke, M. (2016). Solid solution in the apatite OH-Cl binary system: Compositional dependence of solid-solution mechanisms in calcium phosphate apatites along the Cl-OH binary. *American Mineralogist*, 101(8), 1783-1791.
- Hughes, J.M. (2015) The many facets of apatite. Mineralogical Society of America Presidential Address. *American Mineralogist*, 100, 1033–1039.

- Hughes, J. M., Harlov, D., & Rakovan, J. F. (2018). Structural variations along the apatite F-OH join. *American Mineralogist*, 103(12), 1981-1987.
- Jenkins, H.D.B., and Thakur, K.P. (1979) Reappraisal of thermochemical radii for complex anions. *Journal of Chemical Education*, 56, 576–577.
- Kelly, S. R., Rakovan, J., & Hughes, J. M. (2017). Column anion arrangements in chemically zoned ternary chlorapatite and fluorapatite from Kurokura, Japan. *American Mineralogist*, 102(4), 720-727.
- La Fontaine, A., Zavgorodniy, A., Liu, H., Zheng, R., Swain, M., & Cairney, J. (2016). Atomic-scale compositional mapping reveals Mg-rich amorphous calcium phosphate in human dental enamel. *Science Advances*, 2(9), e1601145.
- Luo, Y. R. *Comprehensive Handbook of Chemical Bond Energies*, CRC Press, Boca Raton, FL, 2007.
- Mackie, P.E., and Young, R.A. (1974) Fluorine-chlorine interaction in fluor-chlorapatite. *Journal of Solid State Chemistry*, 11, 319–329.
- Nejad, Z.D., Jung, M. C., and Kim, K.-H. (2018). Remediation of soils contaminated with heavy metals with an emphasis on immobilization technology. *Environmental Geochemistry and Health*, 40(3), 927-953.
- Rigali, Mark J., Brady, Patrick V., & Moore, Robert C.. *Radionuclide removal by apatite*. United States. doi:10.2138/am-2016-5769.
- Sheldrick, G. (2008) A short history of SHELX. *Acta Crystallographica Section A*, 64(1), 112-122.
- Stock, M. J., Humphreys, M. C. S., Smith, V. C., Johnson, R. D., Pyle, D. M., & EIMF. (2015). New constraints on electron-beam induced halogen migration in apatite†. *American Mineralogist*, 100(1), 281-293. *American Mineralogist*
- Stormer, J.C., Pierson, M.L., and Tacker, R.C. (1993) Variation of F and Cl X-ray intensity due to anisotropic diffusion in apatite during electron microprobe analysis. *American Mineralogist*, 78, 641–648.
- Wang, Y., Zhang, L., Hu, M., Liu, H., Wen, W., Xiao, H., & Niu, Y. (2008). Synthesis and characterization of collagen-chitosan-hydroxyapatite artificial bone matrix. *86A(1)*, 244-252.
- Yang, Y.-H., Wu, F.-Y., Yang, J.-H., Chew, D. M., Xie, L.-W., Chu, Z.-Y., Huang, C. (2014). Sr and Nd isotopic compositions of apatite reference materials used in U–Th–Pb geochronology. *Chemical Geology*, 385, 35-55.

Young, R.A., van der Lugt, W., and Elliott, J.C. (1969) Mechanism for fluorine inhibition of diffusion in hydroxyapatite. *Nature*, 223, 729–730.

## Chapter 3: Multiscale Expression of Apatite Dissolution

Conde A, Hellmann R., Rampe E., Christofferson R., Murayama M. and Perdrial N.

*Formatted for submission to Nature Geoscience*

### 3.1 Introduction

The weathering of phosphate minerals is the foundation of the phosphorus cycle and essential to life (Filippelli 2008), yet little is known about the nanoscale mechanisms driving their dissolution. Phosphate minerals have disproportionate importance relative to other mineral classes, in part because phosphorus is required for all life to occur (Adcock et al. 2013). Minerals of the apatite group ( $\text{Ca}_{10}(\text{PO}_4)_6(\text{Cl},\text{F},\text{OH})_2$ ) are the most common of the phosphate minerals on Earth and one of the most common biominerals. Aside from being the primary source of P in the environment, phosphate minerals have many scientific and economic uses in geology, medicine, environmental remediation, and paleoclimatology (Hughes and Rakovan 2015).

Calcium phosphate mineralization and dissolution play an important role in bone and dental decalcification and potential repair (Wang et al. 2008; Ehrlich et al. 2010; Gordon et al. 2015, La Fontaine et al. 2016). Of particular interest, the presence of amorphous domains in bones and teeth can affect their mechanical properties (Gordon et al. 2015). In the context of thermochronology, questions remain as to whether apatite faithfully records thermally-activated diffusion profiles or is influenced by recrystallization and new growth processes and some preconize caution against the use of apatite U-Pb data without detailed knowledge of the grain growth/alteration processes (Kirkland et al. 2018).

Studying the dissolution of phosphate minerals across scales is paramount for understanding and modeling large-scale geochemical regimes. Phosphate minerals,

especially apatite, are amongst the most efficient contaminant scavengers in soils and waters (Nejad et al. 2018; Rigali et al. 2016). Knowledge of apatite stability, precipitation and dissolution mechanisms is crucial to the development of sustainable remediation (Guan et al. 2018). Furthermore, analysis of the isotopic composition of biogenic apatite helps infer past climates, however atomic scale transformations of bones leads to partial dissolution-reprecipitation mechanisms susceptible to modify the fractionation of oxygen isotopes (Aufort et al. 2017).

Recent cutting-edge nanoscale research on the weathering of silicate minerals and glasses has provided compelling evidence of a relatively new chemical weathering mechanism referred to as coupled interfacial dissolution-precipitation (CIDR - Hellmann et al. 2003, 2012, 2015; Putnis and Ruiz-Agudo et al. 2013, 2016). Understanding CIDR mechanisms at the nanoscale is a necessary pre-requisite for predictive numerical modeling of large-scale processes, such as elemental transport through the crust (Putnis, 2014). The CIDR mechanism contradicts the traditional concept of mineral dissolution, the leached layer theory, defined by solid-state interdiffusion of interstitial cation and protons resulting in a sigmoidal elemental gradient through the leached layer (Hellmann et al. 2012). In short, the CIDR mechanism, rather than a leaching process, is defined by the complete dissolution of the mineral occurring at a single reaction front and subsequent partial reprecipitation of dissolution products as a porous and amorphous phase referred to as the surface altered layer (SAL - Hellmann et al. 2012). This discovery is radically improving our understanding of geochemical processes at the molecular scale for silicate minerals (Putnis 2014, 2015), and the extension of CIDR

mechanism to other minerals classes, including phosphate minerals, would imply a paradigm shift in the conceptual framework of mineral weathering.

Similar to silicate minerals, apatite dissolution has been shown to occur under acidic conditions, with a pH dependent rate (Guidry and Mackenzie 2003; Chairat et al. 2007b). Initial apparent preferential Ca release is attributed to apatite-bound Ca being exchanged for solution hydrogen ion during the early stages of the dissolution reaction (Chairat et al. 2007a; Guidry and Mackenzie 2003). Chairat et al. (2007a) further suggested the formation of a P-enriched, Ca-depleted altered layer. SEM analysis has shown etch pits on weathered apatite implying dissolution is not a homogenous process over the surface of the mineral (Chairat et al. 2007b; Harouiya et al. 2007; Valsami-Jones et al. 1998).

Although most of these studies aimed to define the controls on phosphorus availability in aqueous systems, the scale of observation remained “coarse,” with observations performed at the macro- to microscale (cm to  $\mu\text{m}$ ). This study investigates dissolution mechanisms driving Durango fluorapatite (FAP) and hydroxyl-chlorapatite (HAP) across scales with emphasis at the nanoscale using a suite of state-of-the-art techniques.

## **3.2 Materials and Methods**

### **3.2.1 Apatite Characterization**

Prismatic Durango fluorapatite (FAP) and hydroxyl-chlorapatite (HAP) centimetric crystals were acquired from online vendors. Single-crystal X-ray diffraction data was collected on two 80  $\mu\text{m}$  ground spheres for both apatite species to ensure their compositional purity using a Bruker Apex II CCD single-crystal diffractometer equipped

with a graphite-monochromated  $\text{MoK}_\alpha$  radiation. All samples were cleaned with a nanopure  $\text{H}_2\text{O}$ -detergent solution to remove any residual material and then ultrasonically cleaned in a nanopure  $\text{H}_2\text{O}$  bath twice for 5 minutes prior to being dried at ambient temperature. Briefly, the composition of the anion column differed significantly between the apatites with the FAP formula being  $\text{Ca}_{10}(\text{PO}_4)_6(\text{F}_{1.32}\text{OH}_{0.68})$  and the HAP being  $\text{Ca}_{10}(\text{PO}_4)_6(\text{OH}_{1.84}\text{Cl}_{0.16})$ . A subset of the prismatic apatite samples was used to perform controlled dissolution experiments, SEM and FIB-HRTEM analysis.

The apatite sample surface areas were measured optically (<http://nicolasperdrial.weebly.com/tutorials.html>) by taking photos of each individual crystal face with a high-resolution digital camera and analyzing the images with the software ImageJ (Schneider et al. 2012). The relationship between surface area and volume was then estimated to a power function based on the geometric relationship between surface area and volume. A relationship defined by the equation  $\text{SA} = 6.461(v)^{2/3}$ , where SA is surface area, and v is the volume.

### 3.2.2 Dissolution Experiments

Four samples of prismatic FAP and HAP were hydrolyzed at ambient temperature and 1 bar for 6 to 11 days in duplicate in both a 3D printed mixed flow reactor (Michel et al. 2017) and a flow-through column at far from equilibrium conditions. The hydrolyzing solution was composed of 0.001 M omnitrace  $\text{HNO}_3$ -  $\text{H}_2\text{O}$  (pH of 3). All surfaces of the prismatic apatite crystals were in contact with the reactant in free-flowing solution. The flow rate of approximately 0.05 mL/min was controlled by a peristaltic pump and effluent solution was collected in polypropylene vials in 2-hour time increments using a Teledyne Foxy 200 fraction collector (Fig. 3-1).

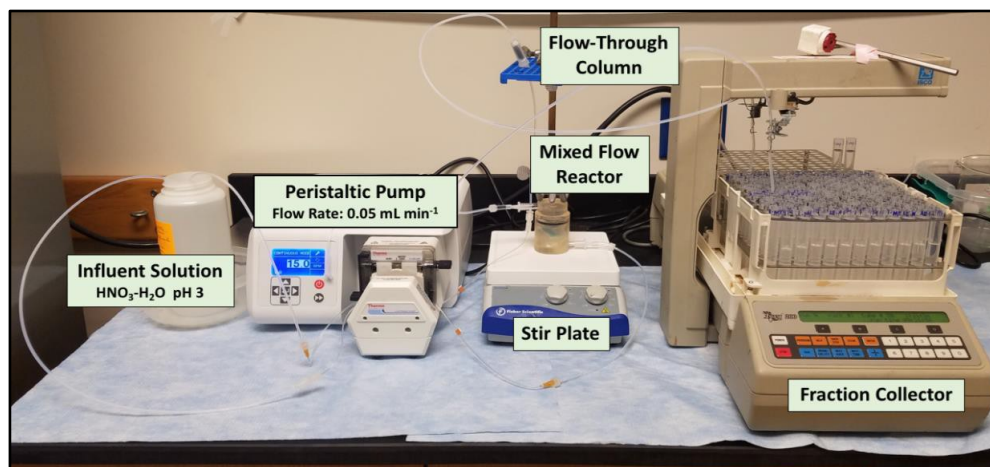


Figure 3-1. Experimental set up of the laboratory dissolution experiments

### 3.2.3 Dissolution Rate and Degree of Undersaturation Calculations

Effluent solutions collected during the dissolution experiments were monitored for pH and analyzed for elemental concentrations of Ca and P using a Jobin Yvon ICP-OES. Effluent concentrations were subsequently converted to stoichiometric-normalized cation release rates ( $R$  expressed in  $\text{mol m}^{-2} \text{s}^{-1}$ ) with respect to the parent mineral composition accounting for sample surface area and flow rate.

The saturation index ( $\text{Log}(Q/K)$ ) of the effluent solution with respect to FAP and HAP and other possible secondary precipitate phases was calculated using the Geochemist Workbench Spec8 modeling software including the LLNL V8 R6 database (Anderson et al. 2000). The equilibrium constants used to calculate the  $\text{log}(Q/K)$  of the solution with respect to FAP and HAP were  $\text{log } K = -49.988$  and  $\text{log } K = -6.1492$  respectively (Robie et al. 1979). Using the calculated  $\text{log } Q/K$ , the Gibbs free energy of the reaction was calculated to determine the degree of undersaturation in the system using  $\Delta G_R = 2.303 R_g T \text{log } \frac{Q}{K}$  where,  $R_g$  is the gas constant ( $1.987 \text{ cal K}^{-1} \text{mol}^{-1}$ ) and  $T$  is temperature (K), and  $\text{Log}(Q/K)$  is the saturation index.

### 3.2.4 SEM and FIB-TEM Analysis:

Images of the crystal surface parallel to the *c*-axis were acquire prior to and following the dissolution experiments using a Tescan Vega 3 LMU SEM at multiple magnifications. For this, individual crystals of both HAP and FAP pre and post dissolution were carbon coated to induce conductivity and observed in SE mode. At least two samples of each apatite were observed.

The nanoscale weathering response was observed using high resolution transmission electron microscopy (HRTEM) and associated energy-dispersive X-ray spectroscopy (EDS) or electron energy loss spectroscopy (EELS), depending on the instrument used. To prepare the samples for HRTEM, a focused ion beam (FIB, Ga<sup>+</sup>) operated at a high beam current was used to mill out a thin electron-transparent lamella of uniform thickness perpendicular to the *c*-axis of the prismatic FAP and HAP samples (for a more detailed description on FIB preparations see Wirth 2004, 2009). FAP and HAP were prepare using slightly different methods depending on the facilities and instrument used for FIB. The HAP cross-section was coated with a thin layer of carbon for contrast prior to FIB milling, and both HAP and FAP cross-sections were coated with a thin layer of platinum to protect them from sputtering by the Ga<sup>+</sup> ion beam during the final stages of the preparation (Wirth, 2009).

The HAP carbon-coated FIB cross-section was prepared on a FEI Quanta 3D FEG and analyzed using a JEM 2500SE TEM and associated EDS at ARES, Johnson Space Center (Houston, TX). Selected areas of the crystal interface were imaged at 200 kV in conventional TEM mode. Chemical maps and profiles were obtained by EDS at

1,000,000 and 1,200,000x magnification using a 1-nm probe, with 0.89 nm spacing between pixels (See appendix a for more details).

The FAP platinum-coated FIB cross-section was performed using a FEI Helios 600 NanoLab and analyzed using a FEI TITAN 300 TEM with associated EELS at NanoEarth Center, Virginia Tech (Blacksburg VA). The FIB cross-section was imaged at high resolution in conventional TEM mode and Scanning TEM- High Angle Annular Dark Field Mode (STEM-HAADF). EELS profiles were acquired using a  $< 90$  pm point-resolution probe with 300 keV electrons along a transverse through the interface between the crystal and the environment. The crystalline character of the material was also determined by Selected Area Electron Diffraction (SAED) (See appendix A for more details).

### 3.3 Results

#### 3.3.1 Macroscale

After 6 to 11 days of weathering, the surfaces of the FAP and HAP samples were visibly altered (Fig. 3-2). Both apatite species were weathered at far-from-equilibrium condition and  $\Delta G_R^\circ$  calculations show that the system was undersaturated with respect to FAP and HAP. The  $\Delta G_R^\circ$  values for the FAP and HAP experiments ranged from -25.1 to -21.5 kJ/mol and -41.9 to -37.2 kJ/mol, respectively.

Dissolution for both apatite species occurred rapidly at the beginning of the experiments and decreased to a dynamic steady-state rate (Fig. 3-3a). Monitoring of the effluent pH and Ca and P concentrations showed that irrespective of the weathering device, after approximately 80-100 hours of reaction FAP and HAP reached dynamic steady-state dissolution rates of  $2.04 \times 10^{-8}$  and  $2.78 \times 10^{-8}$  mol apatite  $m^{-2} s^{-1}$

respectively. The dissolved Ca to P ratio measured throughout the experiment initially showed apparent non-stoichiometric release of Ca with respect to P that became stoichiometric as the system reached pseudo dynamic steady-state (Fig. 3-3b and c), consistent with previous literature on FAP and dental caries in HAP (Vogel et al. 1987; Guidry and Mackenzie 2003; Chairat et al. 2007a). HAP elemental release rates were slightly faster compared to FAP elemental release rates and the pH was buffered more by HAP dissolution than FAP dissolution (Fig. 3-3). No significant difference in dissolution rates was noted between weathering devices.

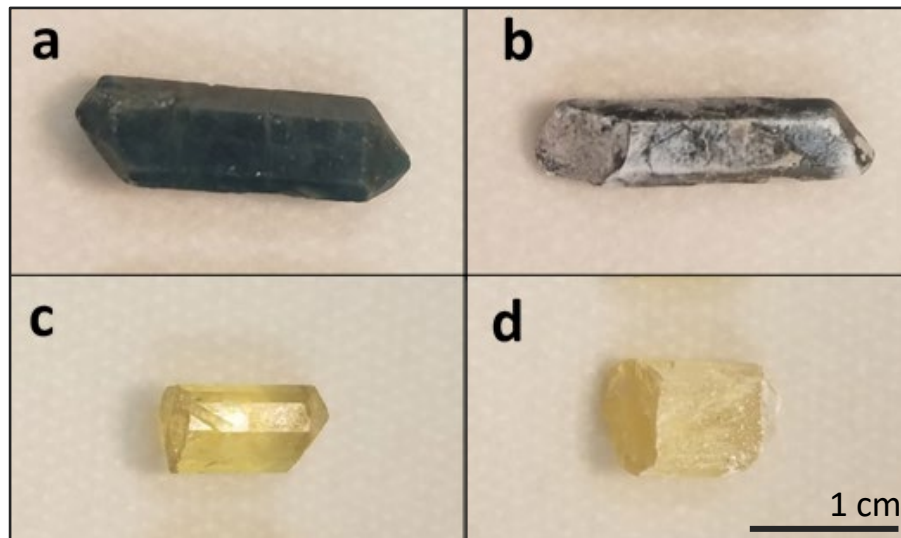


*Figure 3-2. Evidence of surface alteration post-weathering by comparing unaltered a) HAP with c) FAP and weathered b) HAP and d) FAP.*

### **3.3.2 Microscale**

SEM analysis of FAP and HAP surfaces before and after dissolution showed compositional discrepancies in the response to weathering (Fig. 3-4). The surface of weathered FAP samples showed the homogeneous development of elongated, trapezoidal etch pits parallel to the c-axis over the entire mineral surface triggering the development of micrometric “needles” (Fig. 3-4b). In contrast, HAP surfaces showed limited

development of etch pits in localized sites, generally initiated at cracks on the surface of the crystal (Fig. 3-4d).

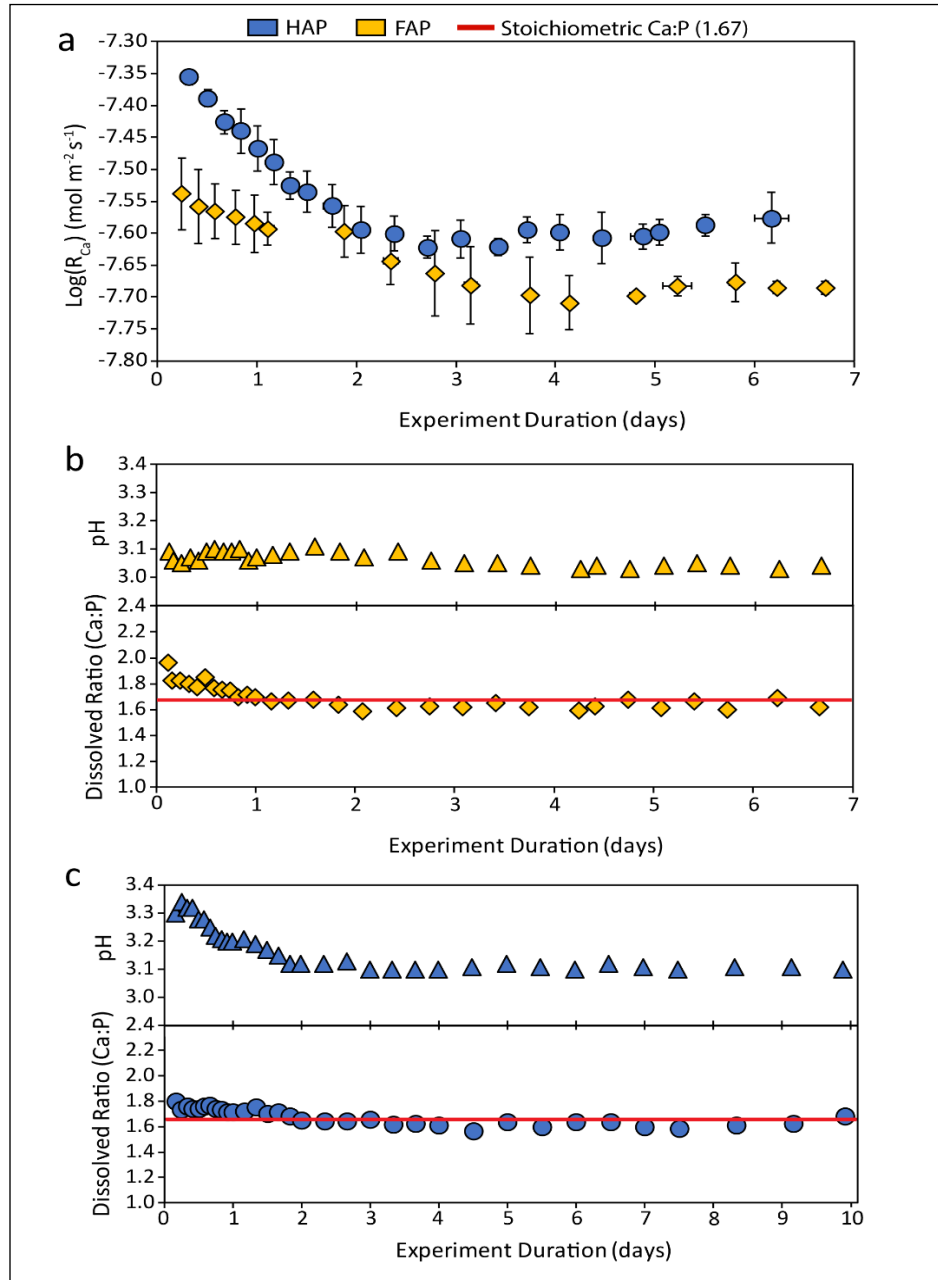
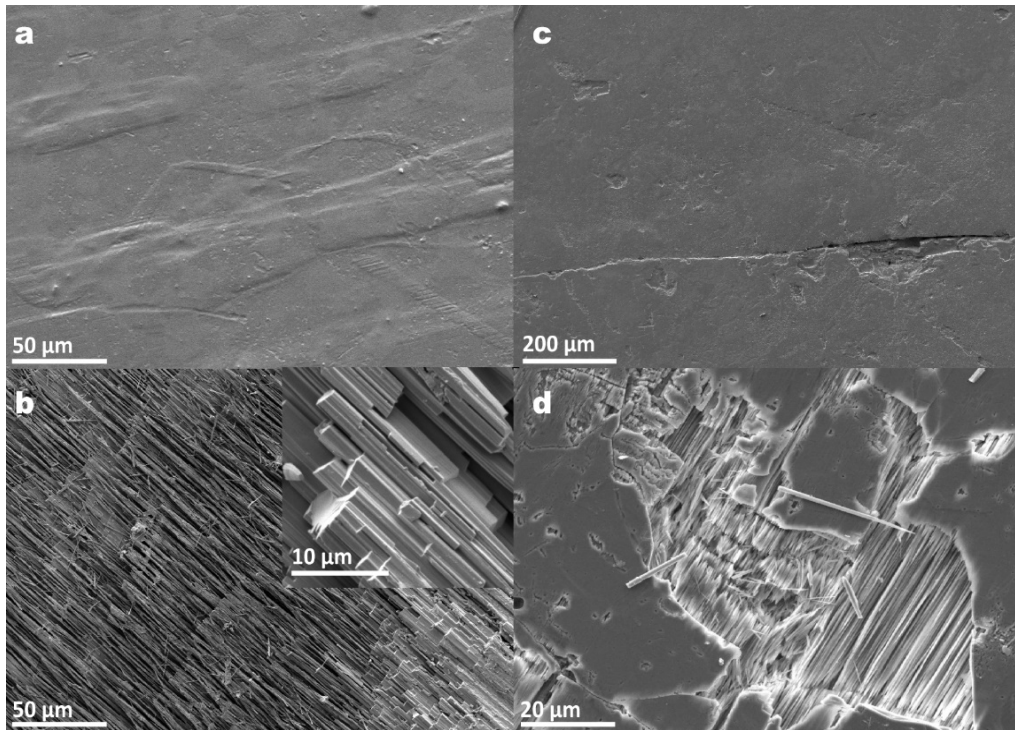


Figure 3-3. a) Evolution of average FAP and HAP Ca-based dissolution rates ( $\log R_{Ca}$  ( $\text{mol m}^{-2} \text{s}^{-1}$ )) as a function of time. b) FAP and c) HAP pH and ratio of dissolved Ca and P throughout weathering of individual experiments. The influent solution was pH 3.04 for HAP and 2.95 for FAP at  $t = 0$  and increased to 3.3 and 3.1 respectively. The red line represents the stoichiometric ratio of Ca:P (1.67) based on the bulk apatite composition. HAP and FAP showed an apparent preferential release of Ca compared to P in the first 24 to 48 hours of reaction, dissolution becoming stoichiometric as the system reached dynamic steady state dissolution.



*Figure 3-4. SEM images of  $10\bar{1}0$  faces of a) fluorapatite before weathering, b) fluorapatite after weathering with detail in inset, c) hydroxyl-chlorapatite before weathering and d) hydroxyl-chlorapatite after weathering.*

### 3.3.3 Nanoscale

As evidenced by the presence and lack of lattice fringes, HRTEM images of the HAP surface displayed a sharp boundary between the unaltered apatite (lattice fringes) and a SAL (absence of fringes) of 5 to 15 nm thick (Fig. 3-5a and b). This SAL was observed across the entire FIB section. Line profiles extracted from EDS chemical maps (Fig. 3-5c and d) showed a gradual Ca depletion in the SAL, while P and O showed a slight enrichment through the SAL (Fig. 3-5e). Approaching the outer boundary, a gradual enrichment of Ca and a depletion of P and O relative to apatites composition was observed. Note that these concentrations are relative, meaning that they always sum to 100.

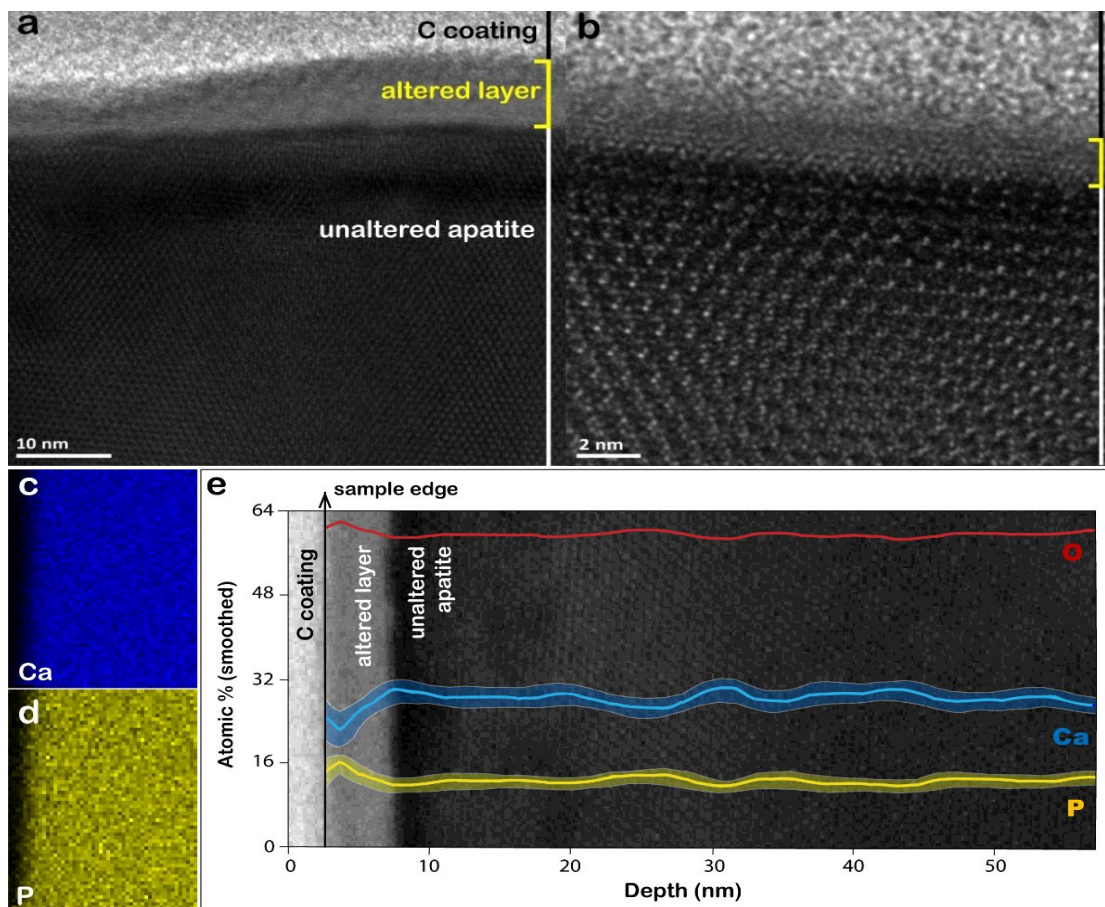


Figure 3-5. *a and b*) Cross-sectional HRTEM images of hydroxyl-chlorapatite showing a nanometric sharp boundary between crystalline unaltered hydroxylapatite (white) and an amorphous surface altered layer (yellow) and a protective coating of carbon (black). Both images were taken on the same FIB prepared cross-section milled perpendicular to the 1010 face. *c and d*) Element maps of Ca and P and *e*) extracted line profile of Ca, P, and O created from EDS compositional spectrum images.

Weathered FAP displayed a relatively sharp boundary between a crystalline domain (lattice fringes, spotted SAED) and a non-crystalline domain (absence of fringes, spotless SAED) identified as a SAL (Fig. 3-6a). The SAL observed on the FAP varied in thickness from 2 to 10 nm. High-resolution EELS profiles taken along multiple transverse from the unaltered apatite to the Pt-coating were inconsistent. While some showed a relatively sharp (< 5 nm) depletion in Ca just before the interface between the unaltered fluorapatite and the SAL (Fig. 3-6b), others showed a similarly sharp relative

enrichment in Ca at the interface (Fig. 3-6c). Additionally, the ratio of Ca to P electron intensities from (Fig. 3-6c) show a Ca enriched SAL (Fig. 3-6d). It should be noted that the Ca enriched EELS profiles were measured in a  $\sim 2$  nm thick region of the SAL, while the EELS profiles that showed a clear Ca depletion in the SAL were measured in a  $\sim 8$  nm thick region.

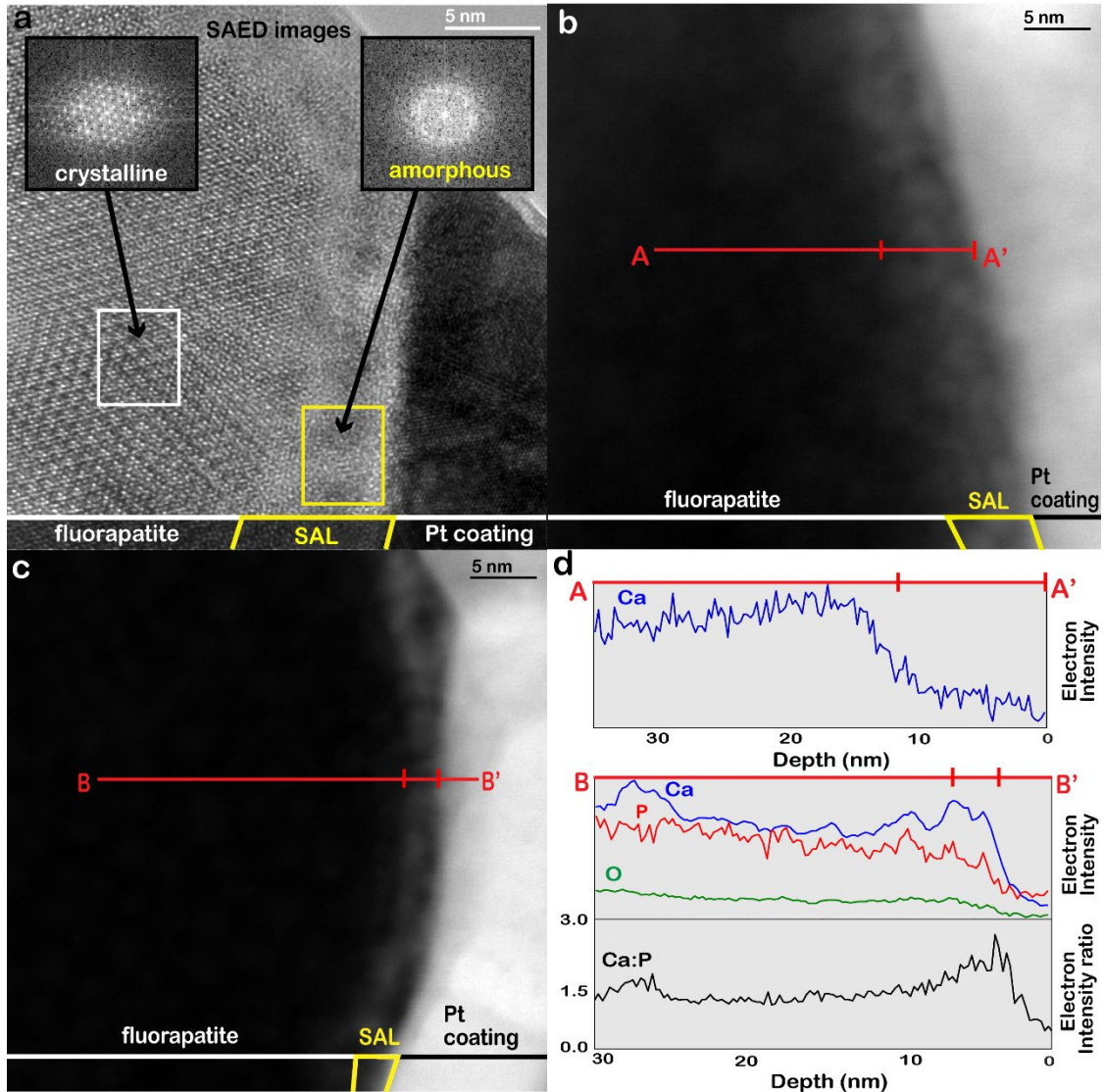


Figure 3-6. a) HRTEM image of the crystal surface of weathered FAP and corresponding SAED patterns. Unaltered, altered and coated layers are identified in the lower end of the image. b) and c) Darkfield HAADF-TEM images of location of EELS Profiles taken along A-A' and B-B' transects (red lines). d) EELS chemical profiles corresponding to A-A' and B-B' transects (red lines) across the interface between the SAL and the unaltered FAP and Ca to P electron intensity ratio across the transect B-B'.

### 3.4 Discussion

Across scales we observed compositionally driven discrepancies in the rate and expression of weathering between FAP and HAP. Our experiments consistently showed a slower dissolution rate for FAP compared to HAP. FAP has a smaller unit cell and stronger bonds in the anion column, which render it less soluble than HAP in the same acidic environment (Adcock 2014).

SEM analysis of unweathered and experimentally weathered HAP and FAP revealed an additional discrepancy. Although HAP weathered at a faster rate than FAP, SEM images consistently showed homogenous development of elongated etch pits on FAP surfaces and limited development of etch pits on HAP surfaces. High dislocation density is often associated with etch pit formation and is likely an important variable in early dissolution (Lagasa et al. 1986; Lee et al. 1998; Rakovan, 2002). HRTEM images did not reveal a significant amount of dislocation in either FAP or HAP.

Our study suggests that anion column homogeneity plays a role in the development of etch pits. Approximately 92% of the HAP anion column is occupied by OH while 33% of the FAP anion column is occupied by OH. Similar to alkali feldspars (Lee et al., 1998), if OH sites have a lower activation energy than F site, the OH sites may preferentially dissolve in the FAP leading uneven weathering features such as etch pits.

Consistent with previous studies, our experiments showed Ca to be released in stoichiometric excess of P for HAP and FAP in the initial stages of the experiments before becoming congruent as the system reaches dynamic steady-state dissolution (Chairat et al. 2007a; 2007b; Gramain et al. 1987; Guidry & Mackenzie 2003; Schaad et al. 1997). Several studies observed this phenomenon and suggested that apparent preferential

release of Ca in the initial stages of FAP and HAP dissolution indicates the formation of a P enrich interfacial layer that slows the elemental release of the apatite (Chairat et al. 2007a; Gramain et al. 1987). However, until recently no direct observation of the SAL existed.

HRTEM images of both FAP and HAP showed the presence of an amorphous SAL, similar, but much thinner, to that observed in silicate minerals (Hellmann et al. 2003, 2012, 2015; Putnis and Ruiz-Agudo et al. 2013, 2016, Fig. 3-3 and 3-4). Based on the initial apparent preferential release of Ca relative to P, the SAL was estimated to be 10 to 30 nm, comparable to the observed thickness of the SAL. The thickness of the SAL was estimated by calculating the area between the Ca dissolution curve ( $\log R_{Ca}$  ( $\text{mol m}^{-2}\text{s}^{-1}$ )) and the P dissolution curve ( $\log R_P$  ( $\text{mol m}^{-2}\text{s}^{-1}$ )) and converting it to thickness using the molar volume of either FAP or HAP. These calculations do not account for variability in the thickness of the SAL, as they assume a SAL of a homogenous thickness across the entire mineral surface.

Optically, the presence of a SAL with sharp transitions is clear. Chemically, however, the sharpness of this transition remains less defined. EDS profiles taken across the SAL/HAP interface indicates that the SAL is relatively Ca depleted and P enriched compared to the unaltered HAP, as suggested by previous studies (Chairat et al. 2007a; Gramain et al. 1987). Comparatively, EELS analysis is better suited to determine the sharpness of the chemical transition at the interface, because of its superior spatial resolution.

Here, EELS profiles taken across the SAL/FAP interface showed that all elements measured decreased in electron density at the interface indicating that the SAL is less

dense than the unaltered FAP. Measurements of Ca in the SAL somewhat disagree as some profiles show a Ca depletion and others show a Ca enrichment. Measuring P in the SAL is difficult due to the size and position of the P energy loss peak. In select regions of the EELS profile the crystalline FAP Ca to P ratio is often higher than stoichiometrically expected (1.67) indicating that P volatilization may be an issue.

Initial apparent preferential release of Ca at the macroscale indicates the formation of a Ca depleted SAL, which is in agreement with previous macroscale observations of initial apparent preferential release of Ca (Chairat et al. 2007a; Guidry and Mackenzie 2003; Vogel et al. 1987). HRTEM-EDS/EELS observations at the nanoscale provide evidence of a Ca depleted and P enriched SAL.

Chairat et al. (2007a) suggests the formation of an altered layer depleted in Ca and enrichment in P via a leached layer mechanism, however, a P enrichment cannot occur via the leached layer mechanism as all chemical elements would decrease in the SAL. P enrichment in the SAL could be explained by the CIDR mechanism as complete dissolution and subsequent reprecipitation could lead to an enrichment in a given element relative to the unaltered mineral. In a companion study, Chairat et al. (2007b) observed that protons may penetrate the surface lattice of FAP, suggesting this occurs through solid-state interdiffusion. Furthermore, they suggest reaching stoichiometric dissolution after initial weathering indicates the destruction of this altered layer.

We observed a SAL after 6 days of dynamic steady-state dissolution *via* HRTEM analysis, suggesting that the initially formed SAL is preserved during weathering. This observation is compatible with stoichiometric dissolution of apatite occurring via aqueous diffusion of proton through a porous SAL. It also suggests that the layer thickness is

maintained during weathering and that, therefore it is not destroyed but rather produced at a rate similar to that of the crystalline apatite dissolution.

Our results suggest that the SAL consist in a Ca-depleted re-precipitated layer covering the crystal in agreement with observations of weathered silicate minerals (CIDR).

### **3.5 Conclusion & Implications**

Direct observation of a SAL with a structurally sharp interface on FAP and HAP *via* HRTEM analysis, combined with macroscale observation of an initial non-stoichiometric dissolution, provides substantial evidence that apatite dissolution is accompanied by the formation of a P enriched and Ca depleted (relative to apatite) SAL. This SAL being preserved *via* reprecipitation throughout the dissolution process. This dissolution mechanism is very similar to the CIDR mechanism now accepted for silicate dissolution. Here, we provide evidence that the CIDR mechanism of dissolution may extend beyond silicates.

This potential ubiquity of the CIDR mechanism has implication for a broad range of fields involving fluid-mineral interactions. As apatite is a ubiquitous mineral occurring in practically every geological setting and even the human body, it is a mineral that regularly experiences these fluid-solid interactions. From metamorphic and weathering reaction to the fluoridation of our tooth enamel, fluid-solid interactions are universally pervasive (Harlov and Austrheim, 2012).

CIDR may help us understand the substitution of OH for F in enamel, as a dissolution-reprecipitation mechanism is thought to control the process (Gregory et al. 1991). Additionally, the discovery of amorphous interfaces in enamel may control

resistance to dissolution and mechanical properties of the hydroxylapatite (Gordon et al. 2015).

At the Earth's surface, weathering of apatite plays an important role in flux of P into the environment, and understanding CIDR will help better determine the rates and inform geochemical models involving P. Observations of silicate dissolution demonstrate that dissolution may be kinetically slowed by the formation of amorphous layer (Daval et al. 2011, 2013, 2017, 2018; Saldi et al. 2015; Wild et al. 2016), formation of a similar "stable" SAL on apatite could pacify weathering, influencing the geochemical modeling of the P cycle.

At greater depths, the CIDR mechanism has implications for thermal, chemical, and structural alteration which inform on the use of apatite and other associated minerals as geochronometers (Betkowski et al. 2016). Monazite inclusions in apatite strongly suggest that apatite can be and has been altered to new compositions during metasomatic alterations via the CIDR mechanism (Harlov et al. 2005; Harlov and Forster 2002, 2003; Harlov et al. 2002a; Harlov et al. 2002b). Many dates determined using apatite likely represent the date of alteration rather than the true geologic age of the mineral (Harrison et al. 2002). Therefore, it is of the utmost importance to understand the mechanisms by which these alterations occur and how to decipher them (Harlov et al. 2005).

### 3.6 References Cited

- Adcock, C. T., E. M. Hausrath and P. M. Forster (2013). "Readily available phosphate from minerals in early aqueous environments on Mars." *Nature Geoscience* 6(10): 824-827.
- Adcock, Christopher (2014). "Mars-Relevant Phosphate Minerals and Implications for Martian Habitability" UNLV Theses, Dissertations, Professional Papers, and Capstones. 2162.
- Aufort, J., Ségalen, L., Gervais, C., Paulatto, L., Blanchard, M., & Balan, E. (2017). Site specific equilibrium isotopic fractionation of oxygen, carbon and calcium in apatite. *Geochimica et Cosmochimica Acta*, 219, 57-73.
- Betkowski, V., Harlov, D. and Rakovan, J. (2016) Hydrothermal mineral replacement reactions for an apatite-monzonite assemblage in alkali-rich fluids at 300-600 OC and 100 MPa. *American Mineralogist*, 101: 2620–2637.
- Chairat, C., Oelkers, E.H., Schott, J. and Lartigue, J.E. (2007a) Fluorapatite surface composition in aqueous solution deduced from potentiometric, electrokinetic, and solubility measurements, and spectroscopic observations. *Geochimica Et Cosmochimica Acta* 71, 5888-5900.
- Chairat, C., Schott, J., Oelkers, E.H., Lartigue, J.E. and Harouiya, N. (2007b) Kinetics and mechanism of natural fluorapatite dissolution at 25 degrees C and pH from 3 to 12. *Geochimica Et Cosmochimica Acta* 71, 5901-5912.
- Daval, D., Bernard, S., Rémusat, L., Wild, B., Guyot, F., Micha, J.S., Rieutord, F., Magnin, V., Fernandez-Martinez, A., (2017). Dynamics of surface altered layer formation on dissolving silicates. *Geochim. Cosmochim. Acta* 209, 51–69.
- Daval, D., Hellmann, R., Saldi, G.D., Wirth, R., Knauss, K.G., (2013). Linking nm-scale measurements of the anisotropy of silicate surface reactivity to macroscopic dissolution rate laws: new insights based on diopside. *Geochim. Cosmochim. Acta* 107, 121–134.
- Daval, D., Sissmann, O., Menguy, N., Saldi, G.D., Guyot, F., Martinez, I., Corvisier, J., Garcia, B., Machouk, I., Knauss, K.G., Hellmann, R., (2011). Influence of amorphous silica layer formation on the dissolution rate of olivine at 90 degrees C and elevated pCO<sub>2</sub>. *Chem. Geol.* 284, 193–209.
- Drouet, C. (2015). A comprehensive guide to experimental and predicted thermodynamic properties of phosphate apatite minerals in view of applicative purposes. *The Journal of Chemical Thermodynamics*, 81, 143-159.

- Ehrlich, H., Hanke, T., Born, R., Fischer, C., Frolov, A., Langrock, T., Worch, H. (2009). Mineralization of biomimetically carboxymethylated collagen fibrils in a model dual membrane diffusion system. *Journal of Membrane Science*, 326(2), 254-259.
- Ewing, R.C., and Wang, L. (2002) Phosphates as nuclear waste forms. *Reviews in Mineralogy and Geochemistry*, 48, 673–700.
- Filippelli, G.M. (2008) The global phosphorus cycle: Past, present, and future. *Elements* 4, 89-95.
- Geisler, T., Nagel, T., Kilburn, M. R., Janssen, A., Icenhower, J. P., Fonseca, R. O. C., Nemchin, A. A. (2015). The mechanism of borosilicate glass corrosion revisited. *Geochimica et Cosmochimica Acta*, 158, 112-129.
- Geisler T., Janssen A., Scheiter D., Stephan T., Berndt J. and Putnis A. (2010) Aqueous corrosion of borosilicate glass under acidic conditions: a new corrosion mechanism. *J. Non-Cryst. Solids* 356, 1458–1465.
- Gordon, L. M., Cohen, M. J., MacRenaris, K. W., Pasteris, J. D., Seda, T., & Joester, D. (2015) Amorphous intergranular phases control the properties of rodent tooth enamel. *Science*, 347(6223), 746. doi:10.1126/science.1258950
- Gramain, P. H., Thomann, J. M., Gumpfer, M., & Voegel, J. C. (1989) Dissolution kinetics of human enamel powder: I. Stirring effects and surface calcium accumulation. *Journal of Colloid and Interface Science*, 128(2), 370-381.
- Grant, T.B., Milke, R., Wunder, B., Wirth, R. and Rhede, D. (2014) Experimental study of phlogopite reaction rim formation on olivine in phonolite melts: Kinetics, reaction rates, and residence times. *American Mineralogist* 99, 2211-2226
- Gregory, T. M., Chow, L. C., & Carey, C. M. (1991) A Mathematical Model for Dental Caries: A Coupled Dissolution-Diffusion Process. *Journal of research of the National Institute of Standards and Technology*, 96(5), 593–604.
- Guan, D.-X., Ren, C., Wang, J., Zhu, Y., Zhu, Z., & Li, W., (2018) Characterization of Lead Uptake by Nano-Sized Hydroxyapatite: A Molecular Scale Perspective. *ACS Earth and Space Chemistry*, 2(6), 599-607.
- Guidry, M.W. and Mackenzie, F.T. (2003) Experimental study of igneous and sedimentary apatite dissolution: Control of pH, distance from equilibrium, and temperature on dissolution rates. *Geochimica Et Cosmochimica Acta* 67, 2949-2963.

- Harlov, D. & Austrheim, H., (2013) Metasomatism and the chemical transformation of rock: rock-mineral-fluid interaction in terrestrial and extraterrestrial environments. In: *Metasomatism and the Chemical Transformation of Rock* (eds D. Harlov & H. Austrheim), pp. 1– 16. Springer-Verlag, Berlin, Heidelberg.
- Harlov DE, Forster H-J, Nijland TG (2002a) Fluid-induced nucleation of REE-phosphate minerals in apatite: nature and experiment. Part I. Chlorapatite *Am Mineral* 87:245–261
- Harlov DE, Andersson UB, Forster H-J, Nystrom JO, Dulski P, Broman C (2002b) Apatite-monazite relations in the Kiirunavaara magnetite-apatite ore, northern Sweden *Chem Geol* 191:47–72
- Harlov DE, Forster H-J (2003) Fluid-induced nucleation of REE phosphate minerals in apatite: nature and experiment. Part II. Fluorapatite *Am Mineral* 88:1209–1229
- Harouiya, N., Chairat, C., Köhler, S. J., Gout, R., & Oelkers, E. H. (2007). The dissolution kinetics and apparent solubility of natural apatite in closed reactors at temperatures from 5 to 50 °C and pH from 1 to 6. *Chemical Geology*, 244(3-4), 554-568.
- Harrison TM, Catlos EJ, Montel J-M (2002) U–Th–Pb dating of phosphate minerals. *Rev Mineral Geochem* 48:523–558
- Hellmann, R., Cotte, S., Cadel, E., Malladi, S., Karlsson, L.S., Lozano-Perez, S., Cabie, M. and Seyeux, A. (2015) Nanometre-scale evidence for interfacial dissolution-reprecipitation control of silicate glass corrosion. *Nature Materials* 14, 307-311.
- Hellmann, R., Wirth, R., Daval, D., Barnes, J.P., Penisson, J.M., Tisserand, D., Epicier, T., Florin, B. and Hervig, R.L. (2012) Unifying natural and laboratory chemical weathering with interfacial dissolution-reprecipitation: A study based on the nanometer-scale chemistry of fluid silicate interfaces. *Chemical Geology* 294, 203-216.
- Hellmann, R., Penisson, J.M., Hervig, R.L., Thomassin, J.H. and Abrioux, M.F. (2003) An EFTEM/HRTEM high-resolution study of the near surface of labradorite feldspar altered at acid pH: evidence for interfacial dissolution-reprecipitation. *Physics and Chemistry of Minerals* 30, 192-197.
- Hellmann, R. (1994) The Albite-Water System .1. The Kinetics of dissolution as a Function of pH at 100-Degrees-C, 200-Degrees-C, 300-Degrees-C. *Geochimica Et Cosmochimica Acta* 58, 595-611.

- Hellmann, R. (1995) The Albite-Water System .2. The Time-Evolution of The Stoichiometry of Dissolution as a Function of pH at 100-Degrees-C, 200-Degrees-C, 300-Degrees-C. *Geochimica Et Cosmochimica Acta* 59, 1669-1697.
- Hughes, J.M. (2015) The many facets of apatite. Mineralogical Society of America Presidential Address. *American Mineralogist*, 100, 1033–1039.
- Hughes, J.M. and Rakovan, J.F. (2015) Structurally Robust, Chemically Diverse: Apatite and Apatite Supergroup Minerals. *Elements* 11, 165-170.
- Johnson, J., Anderson, F., Parkhurst,DL., (2000) Database thermo.com.V8.R6.230, Rev 1.11. Lawrence Livermore National Laboratory, Livermore, California
- Kirkland, C. L., Yakymchuk, C., Szilas, K., Evans, N., Hollis, J., McDonald, B., & Gardiner, N. J. (2018). Apatite: a U-Pb thermochronometer or geochronometer? *Lithos*, 318-319, 143-157.
- La Fontaine, A., Zavgorodniy, A., Liu, H., Zheng, R., Swain, M., & Cairney, J. (2016). Atomic-scale compositional mapping reveals Mg-rich amorphous calcium phosphate in human dental enamel. *Science Advances*, 2(9), e1601145.
- Lasaga A. C. and Blum A. E. (1986) Surface chemistry, etch pits and mineral-water reactions. *Geochim. Cosmochim. Acta* 50, 2363–2379.
- Lee M. R., Hodson M. E., and Parsons I. (1998) The role of intragranular microtexture and microstructures in chemical and mechanical weathering: Direct comparisons of experimentally and naturally weathered alkali feldspars. *Geochim. Cosmochim. Acta* 62, 2771–2788.
- Maher, K., Steefel, C.I., DePaolo, D.J. and Viani, B.E. (2006) The mineral dissolution rate conundrum: Insights from reactive transport modeling of U isotopes and pore fluid chemistry in marine sediments. *Geochimica Et Cosmochimica Acta* 70, 337-363.
- Michel, F. M., J. D. Rimstidt and K. Kletetschka (2018). 3D printed mixed flow reactor for geochemical rate measurements. *Applied Geochemistry* 89: 86-91.
- Muir, I.J., Bancroft, G.M. and Nesbitt, H.W. (1989) Characteristics of Altered Labradorite Surfaces by SIM and *Geochimica Et Cosmochimica Acta* 53, 1235-1241.
- Nejad, Z.D., Jung, M. C., and Kim, K.-H. (2018). Remediation of soils contaminated with heavy metals with an emphasis on immobilization technology. *Environmental Geochemistry and Health*, 40(3), 927-953.

- Noiriel, C., Steefel, C.I., Yang, L. and Ajo-Franklin, J. (2012) Upscaling calcium carbonate precipitation rates from pore to continuum scale. *Chemical Geology* 318, 60-74.
- Oelkers, E.H. and Valsami-Jones, E (2008). Phosphate Mineral Reactivity and Global Sustainability. *Elements* 4(2): 83-87.
- O'Neil, J.R. and Taylor, H.P.J. (1967) The oxygen isotope and cation exchange chemistry of feldspars. *American Mineralogist* 52, 1414-1437.
- Parsons, I., Lee, M. R., & Smith, J. V. (1998). Biochemical evolution II: Origin of life in tubular microstructures on weathered feldspar surfaces. *Proceedings of the National Academy of Sciences*, 95(26), 15173
- Putnis A (2002) Mineral replacement reactions: from macroscopic observations to microscopic mechanisms *Mineral Mag* 66:689–708
- Putnis, A., & Putnis, C. V. (2007). The mechanism of reequilibration of solids in the presence of a fluid phase. *Journal of Solid-State Chemistry*, 180(5), 1783-1786.
- Putnis, C.V. and Ruiz-Agudo, E. (2013) The Mineral-Water Interface: Where Minerals React with the Environment. *Elements* 9, 177-182.
- Putnis, A. (2014) Why Mineral Interfaces Matter. *Science* 343, 1441-1442.
- Putnis, A. (2015) Sharpened interface. *Nature Materials* 14, 261-262.
- Putnis, A. (2016) Control of silicate weathering by interface-coupled dissolution-precipitation processes at the mineral-solution interface. *Geology* 44, 567-570.
- Rakovan, J. (2002). "Growth and Surface Properties of Apatite." *Reviews in Mineralogy and Geochemistry* 48(1): 51-86.
- Rigali, Mark J., Brady, Patrick V., & Moore, Robert C.. *Radionuclide removal by apatite*. United States. doi:10.2138/am-2016-5769.
- Robie R. A., Hemingway B. S., and Fisher J. R. (1979) Thermodynamic properties of minerals and related substances at 298.15K and 1 bar (105 Pascals) pressure and at higher temperatures: U.S.G.S. Bull. 1452 (with corrections). **1452**, 1456p.
- Ruiz-Agudo, E., King, H.E., Patino-Lopez, L.D., Putnis, C.V., Geisler, T., Rodriguez-Navarro, C. and Putnis, A. (2016) Control of silicate weathering by interface-coupled dissolution precipitation processes at the mineral-solution interface. *Geology* 44, 567-570.
- Ruiz-Agudo, E., Putnis, C.V. and Putnis, A. (2014) Coupled dissolution and precipitation at mineral-fluid interfaces. *Chemical Geology* 383, 132-146.

- Ruiz-Agudo, E., Putnis, C.V., Rodriguez-Navarro, C., Putnis, A., 2012. Mechanism of leached layer formation during chemical weathering of silicate minerals. *Geology* 40, 947–950.
- Saldi, G.D., Daval, D., Guo, H., Guyot, F., Bernard, S., Le Guillou, C., Davis, J.A., Knauss, K.G., 2015. Mineralogical evolution of Fe–Si-rich layers at the olivine–water in-interface during carbonation reactions. *Am. Mineral.* 100, 2655–2669.
- Saldi, G.D., Daval, D., Guo, H., Guyot, F., Bernard, S., Le Guillou, C., Davis, J.A., Knauss, K.G., 2015. Mineralogical evolution of Fe–Si-rich layers at the olivine–water in-interface during carbonation reactions. *Am. Mineral.* 100, 2655–2669.
- Schaad Ph., Poumier F., Voegel J. C., and Gramain Ph. (1997) Analysis of calcium hydroxyapatite dissolution in non-stoichiometric solutions. *Coll. Surf. A: Physicochem. Eng. Asp.* **121**, 217–228.
- Schneider, C. A.; Rasband, W. S. & Eliceiri, K. W. (2012), "NIH Image to ImageJ: 25 years of image analysis", *Nature methods* **9**(7): 671-675.
- Schwartz, A. W., (2006) Phosphorus in Prebiotic Chemistry: *Philosophical Transactions: Biological Sciences*, v. 361, no. 1474, p. 1743-1749.
- Valsami-Jones, E., Ragnarsdottir, K.V., Putnis, A., Bosbach, D., Kemp, A.J. and Cressey, G. (1998) The dissolution of apatite in the presence of aqueous metal cations at pH 2-7. *Chemical Geology* 151, 215-233.
- Vogel, G. L., Carey, C. M., Chow, L. C., Gregory, T. M., & Brown, W. E. (1987). Ultramicro Analysis of the Fluid in Human Enamel During in vitro Caries Attack by Hydrochloric Acid. *Caries Research*, 21(4), 310-325.
- Wang, Y., Zhang, L., Hu, M., Liu, H., Wen, W., Xiao, H., & Niu, Y. (2008). Synthesis and characterization of collagen-chitosan-hydroxyapatite artificial bone matrix. *86A*(1), 244-252.
- Wild, B., Daval, D., Guyot, F., Knauss, K.G., Pollet-Villard, M., Imfeld, G., 2016. pH-dependent control of feldspar dissolution rate by surface altered layers. *Chem. Geol.* 442, 148–159.
- Wirth, R., 2004. Focused Ion Beam (FIB): a novel technology for advanced application of micro- and nanoanalysis in geosciences and applied mineralogy. *European Journal of Mineralogy* 16, 863–876.
- Wirth, R., 2009. Focused Ion Beam (FIB) combined with SEM and TEM: advanced analytical tools for studies of chemical composition, microstructure and crystal structure in geomaterials on a nanometre scale. *Chemical Geology* 261, 217–229.

Zhu, Y., Zhang X., Chen Y., Xie Q., Lan J., Qian M., He N., (2009). "A comparative study on the dissolution and solubility of hydroxylapatite and fluorapatite at 25°C and 45°C." *Chemical Geology* 268(1): 89-96.

## Chapter 4: Conclusions and Future Work

Apatite occurs in every geologic setting and is one of the most common biominerals on Earth. The availability of P through weathering of apatite is a process indispensable to life. Apatite stability has implications for teeth and bone demineralization and remineralization, sustainability of heavy metal and radionuclide sequestration via apatite, and the accuracy of geochronologic apatite records.

Observations of apatite dissolution demonstrate that the primary control lies in the anionic composition. This study consistently showed that hydroxyl-chlorapatite (HAP) weathered faster than Durango fluorapatite (FAP), as expected based on the larger atomic size of OH and Cl compared to F (Jenkins and Thakur 1979) and derived bond strength. Apatite solubility and dissolution processes likely depend heavily on the mechanisms by which solid-solution exists in the column anion column. Therefore, understanding how solid-solution exists in the anion column of apatite is vital for studying its dissolution.

Furthermore, this work provides new evidence that the CIDR mechanism of dissolution extends beyond silicates, based on direct observation of a SAL with a structurally sharp interface on FAP and HAP and initial apparent non-stoichiometric dissolution at the macroscale. We suggest that the SAL is preserved *via* reprecipitation throughout the dissolution process.

Future studies on the CIDR mechanism in apatite should focus on determining the sharpness of the chemical boundary at the interface between the pristine apatite and the SAL. Previous studies have shown SAL thickness to be dependent on flow rate, with thicker SAL forming at lower flow rates (Hellmann et al. 2012; Ruiz-Agudo et al. 2016). The thin SAL observed on the HAP and FAP could be partially due to the relatively high

fluid flow rates. To simplify characterization of the SAL and the SAL/FAP boundary dissolution experiments should be set up with the final SAL thickness in mind.

## Chapter 5: Comprehensive Bibliography

- Adcock, C. T., E. M. Hausrath and P. M. Forster (2013). "Readily available phosphate from minerals in early aqueous environments on Mars." *Nature Geoscience* 6(10): 824-827.
- Adcock, Christopher (2014). "Mars-Relevant Phosphate Minerals and Implications for Martian Habitability" UNLV Theses, Dissertations, Professional Papers, and Capstones. 2162.
- Altree-Williams, A., Pring, A., Ngothai, Y. and Brugger, J. (2015) Textural and compositional complexities resulting from coupled dissolution–reprecipitation reactions in geomaterials. *Earth-Science Reviews* 150, 628-651.
- Aufort, J., Ségalen, L., Gervais, C., Paulatto, L., Blanchard, M., & Balan, E. (2017). Site specific equilibrium isotopic fractionation of oxygen, carbon and calcium in apatite. *Geochimica et Cosmochimica Acta*, 219, 57-73.
- Banfield, J.F., Jones, B.F. and Veblen, D.R. (1991) An AFM-TEM Study of Weathering and Diagenesis, Abert Lake, Oregon .1. Weathering Reactions in The Volcanics. *Geochimica Et Cosmochimica Acta* 55, 2781-2793.
- Batkowski, V., Harlov, D. and Rakovan, J. (2016) Hydrothermal mineral replacement reactions for an apatite-monzonite assemblage in alkali-rich fluids at 300-600 OC and 100 MPa. *American Mineralogist*, 101: 2620–2637.
- Breese, N.E., and O’Keeffe, M. (1991) Bond-valence parameters for solids. *Acta Crystallographica*, B47, 192–197.
- Cappelli, C., Lamarca-Irisarri, D., Camas, J., Huertas, F.J. and Van Driessche, A.E.S. (2015) In situ observation of biotite (001) surface dissolution at pH 1 and 9.5 by advanced optical microscopy. *Beilstein Journal of Nanotechnology* 6, 665-673.
- Casey W. H., Westrich H. R., Banfield J. F., Ferruzzi G. and Arnold G. W. (1993) Leaching and reconstruction at the surfaces of dissolving chain-silicate minerals. *Nature* 366, 253–256.
- Casey, W.H., Westrich, H.R. and Arnold, G.W. (1988) Surface-Chemistry of Labradorite Feldspar Reacted with Aqueous-Solutions at pH =2, 3, and 12.. *Geochimica Et Cosmochimica Acta* 52, 2795-2807.
- Chadwick, O. A., Derry, L. A., Vitousek, P. M., Huebert, B. J., and Hedin, L. O., (1999). Changing sources of nutrients during four million years of ecosystem development: *Nature (London)*, v. 397, no. 6719, p. 491-497.

- Chairat, C., Oelkers, E.H., Schott, J. and Lartigue, J.E. (2007a) Fluorapatite surface composition in aqueous solution deduced from potentiometric, electrokinetic, and solubility measurements, and spectroscopic observations. *Geochimica Et Cosmochimica Acta* 71, 5888-5900.
- Chairat, C., Schott, J., Oelkers, E.H., Lartigue, J.E. and Harouiya, N. (2007b) Kinetics and mechanism of natural fluorapatite dissolution at 25 degrees C and pH from 3 to 12. *Geochimica Et Cosmochimica Acta* 71, 5901-5912.
- Clark, C. M. (2016). Single-crystal Structure Refinement (SREF). Retrieved from [https://serc.carleton.edu/research\\_education/geochemsheets/SREF.html](https://serc.carleton.edu/research_education/geochemsheets/SREF.html)
- Constantz, B.R., and Osaka, G.C. (1994) Hydroxyapatite prosthesis coatings. U.S. Patent 5,279,831 A.
- Cordell, D., Drangert, J.-O. and White, S. (2009) The story of phosphorus: Global food security and food for thought. *Global Environmental Change* 19, 292-305.
- Daval, D., Bernard, S., Rémusat, L., Wild, B., Guyot, F., Micha, J.S., Rieutord, F., Magnin, V., Fernandez-Martinez, A., (2017). Dynamics of surface altered layer formation on dissolving silicates. *Geochim. Cosmochim. Acta* 209, 51–69.
- Daval, D., Hellmann, R., Saldi, G.D., Wirth, R., Knauss, K.G., (2013). Linking nm-scale measurements of the anisotropy of silicate surface reactivity to macroscopic dissolution rate laws: new insights based on diopside. *Geochim. Cosmochim. Acta* 107, 121–134.
- Daval, D., Sissmann, O., Menguy, N., Saldi, G.D., Guyot, F., Martinez, I., Corvisier, J., Garcia, B., Machouk, I., Knauss, K.G., Hellmann, R., (2011). Influence of amorphous silica layer formation on the dissolution rate of olivine at 90 degrees C and elevated pCO<sub>2</sub>. *Chem. Geol.* 284, 193–209.
- Drouet, C. (2015). A comprehensive guide to experimental and predicted thermodynamic properties of phosphate apatite minerals in view of applicative purposes. *The Journal of Chemical Thermodynamics*, 81, 143-159.
- Ehrlich, H., Hanke, T., Born, R., Fischer, C., Frolov, A., Langrock, T., Worch, H. (2009). Mineralization of biomimetically carboxymethylated collagen fibrils in a model dual membrane diffusion system. *Journal of Membrane Science*, 326(2), 254-259.
- Ewing, R.C., and Wang, L. (2002) Phosphates as nuclear waste forms. *Reviews in Mineralogy and Geochemistry*, 48, 673–700.
- Filippelli, G. M., 2002, The Global Phosphorus Cycle: Reviews in Mineralogy and Geochemistry, v. 48, no. 1, p. 391-425.

- Filippelli, G.M. (2008) The global phosphorus cycle: Past, present, and future. *Elements* 4, 89-95.
- Geisler, T., Nagel, T., Kilburn, M. R., Janssen, A., Icenhower, J. P., Fonseca, R. O. C., Nemchin, A. A. (2015). The mechanism of borosilicate glass corrosion revisited. *Geochimica et Cosmochimica Acta*, 158, 112-129.
- Geisler T., Janssen A., Scheiter D., Stephan T., Berndt J. and Putnis A. (2010) Aqueous corrosion of borosilicate glass under acidic conditions: a new corrosion mechanism. *J. Non-Cryst. Solids* 356, 1458–1465.
- Gordon, L. M., Cohen, M. J., MacRenaris, K. W., Pasteris, J. D., Seda, T., & Joester, D. (2015) Amorphous intergranular phases control the properties of rodent tooth enamel. *Science*, 347(6223), 746. doi:10.1126/science.1258950
- Gramain, P. H., Thomann, J. M., Gumpfer, M., & Voegel, J. C. (1989) Dissolution kinetics of human enamel powder: I. Stirring effects and surface calcium accumulation. *Journal of Colloid and Interface Science*, 128(2), 370-381.
- Grant, T.B., Milke, R., Wunder, B., Wirth, R. and Rhede, D. (2014) Experimental study of phlogopite reaction rim formation on olivine in phonolite melts: Kinetics, reaction rates, and residence times. *American Mineralogist* 99, 2211-2226
- Gregory, T. M., Chow, L. C., & Carey, C. M. (1991) A Mathematical Model for Dental Caries: A Coupled Dissolution-Diffusion Process. *Journal of research of the National Institute of Standards and Technology*, 96(5), 593–604.
- Guan, D.-X., Ren, C., Wang, J., Zhu, Y., Zhu, Z., & Li, W., (2018) Characterization of Lead Uptake by Nano-Sized Hydroxyapatite: A Molecular Scale Perspective. *ACS Earth and Space Chemistry*, 2(6), 599-607.
- Guidry, M.W. and Mackenzie, F.T. (2003) Experimental study of igneous and sedimentary apatite dissolution: Control of pH, distance from equilibrium, and temperature on dissolution rates. *Geochimica Et Cosmochimica Acta* 67, 2949-2963.
- Harlov, D. & Austrheim, H., (2013) Metasomatism and the chemical transformation of rock: rock-mineral-fluid interaction in terrestrial and extraterrestrial environments. In: *Metasomatism and the Chemical Transformation of Rock* (eds D. Harlov & H. Austrheim), pp. 1– 16. Springer-Verlag, Berlin, Heidelberg.
- Harlov DE, Forster H-J, Nijland TG (2002a) Fluid-induced nucleation of REE-phosphate minerals in apatite: nature and experiment. Part I. Chlorapatite *Am Mineral* 87:245–261

- Harlov DE, Andersson UB, Forster H-J, Nystrom JO, Dulski P, Broman C (2002b) Apatite-monazite relations in the Kiirunavaara magnetite-apatite ore, northern Sweden *Chem Geol* 191:47–72
- Harlov DE, Forster H-J (2003) Fluid-induced nucleation of REE phosphate minerals in apatite: nature and experiment. Part II. Fluorapatite *Am Mineral* 88:1209–1229
- Harouiya, N., Chairat, C., Köhler, S. J., Gout, R., & Oelkers, E. H. (2007). The dissolution kinetics and apparent solubility of natural apatite in closed reactors at temperatures from 5 to 50 °C and pH from 1 to 6. *Chemical Geology*, 244(3-4), 554-568.
- Harrison TM, Catlos EJ, Montel J-M (2002) U–Th–Pb dating of phosphate minerals. *Rev Mineral Geochem* 48:523–558
- Hawthorne, F.C., and Grice, J.D. (1990) Crystal-structure analysis as a chemical analytical method: application to light elements. *Canadian Mineralogist*, 28, 693–702.
- Hellmann, R., Cotte, S., Cadel, E., Malladi, S., Karlsson, L.S., Lozano-Perez, S., Cabie, M. and Seyeux, A. (2015) Nanometre-scale evidence for interfacial dissolution-reprecipitation control of silicate glass corrosion. *Nature Materials* 14, 307-311.
- Hellmann, R., Wirth, R., Daval, D., Barnes, J.P., Penisson, J.M., Tisserand, D., Epicier, T., Florin, B. and Hervig, R.L. (2012) Unifying natural and laboratory chemical weathering with interfacial dissolution-reprecipitation: A study based on the nanometer-scale chemistry of fluid silicate interfaces. *Chemical Geology* 294, 203-216.
- Hellmann, R., Penisson, J.M., Hervig, R.L., Thomassin, J.H. and Abrioux, M.F. (2003) An EFTEM/HRTEM high-resolution study of the near surface of labradorite feldspar altered at acid pH: evidence for interfacial dissolution-reprecipitation. *Physics and Chemistry of Minerals* 30, 192-197.
- Hellmann, R. (1994) The Albite-Water System .1. The Kinetics of dissolution as a Function of pH at 100-Degrees-C, 200-Degrees-C, 300-Degrees-C. *Geochimica Et Cosmochimica Acta* 58, 595-611
- Hellmann, R. (1995) The Albite-Water System .2. The Time-Evolution of The Stoichiometry of Dissolution as a Function of pH at 100-Degrees-C, 200-Degrees-C, 300-Degrees-C. *Geochimica Et Cosmochimica Acta* 59, 1669-1697.
- Hughes, J.M., Cameron, M., and Crowley, K.D. (1990) Crystal structures of natural ternary apatites: solid solution in the  $\text{Ca}_5(\text{PO}_4)_3\text{X}$  (X = F, OH, Cl) system. *American Mineralogist*, 75, 295–304.

- Hughes, J.M., Nekvasil, H., Ustunisik, G., Lindsley, D.H., Coraor, A.E., Vaughn, J., Phillips, B., McCubbin, F.M., and Woerner, W.R. (2014) Solid solution in the fluorapatite-chlorapatite binary system: High-precision crystal structure refinements of synthetic F-Cl apatite. *American Mineralogist*, 99, 369–376.
- Hughes, J.M. (2015) The many facets of apatite. Mineralogical Society of America Presidential Address. *American Mineralogist*, 100, 1033–1039.
- Hughes, J.M. and Rakovan, J.F. (2015) Structurally Robust, Chemically Diverse: Apatite and Apatite Supergroup Minerals. *Elements* 11, 165-170.
- Hughes, J. M., Harlov, D., Kelly, S. R., Rakovan, J., & Wilke, M. (2016). Solid solution in the apatite OH-Cl binary system: Compositional dependence of solid-solution mechanisms in calcium phosphate apatites along the Cl-OH binary. *American Mineralogist*, 101(8), 1783-1791.
- Hughes, J. M., Harlov, D., & Rakovan, J. F. (2018). Structural variations along the apatite F-OH join. *American Mineralogist*, 103(12), 1981-1987.
- Jenkins, H.D.B., and Thakur, K.P. (1979) Reappraisal of thermochemical radii for complex anions. *Journal of Chemical Education*, 56, 576–577.
- Johnson, J., Anderson, F., Parkhurst, D.L., (2000) Database thermo.com.V8.R6.230, Rev 1.11. Lawrence Livermore National Laboratory, Livermore, California
- Kelly, S. R., Rakovan, J., & Hughes, J. M. (2017). Column anion arrangements in chemically zoned ternary chlorapatite and fluorapatite from Kurokura, Japan. *American Mineralogist*, 102(4), 720-727.
- Kirkland, C. L., Yakymchuk, C., Szilas, K., Evans, N., Hollis, J., McDonald, B., & Gardiner, N. J. (2018). Apatite: a U-Pb thermochronometer or geochronometer? *Lithos*, 318-319, 143-157.
- La Fontaine, A., Zavgorodniy, A., Liu, H., Zheng, R., Swain, M., & Cairney, J. (2016). Atomic-scale compositional mapping reveals Mg-rich amorphous calcium phosphate in human dental enamel. *Science Advances*, 2(9), e1601145.
- Lasaga A. C. and Blum A. E. (1986) Surface chemistry, etch pits and mineral-water reactions. *Geochim. Cosmochim. Acta* 50, 2363–2379.
- Lee M. R., Hodson M. E., and Parsons I. (1998) The role of intragranular microtexture and microstructures in chemical and mechanical weathering: Direct comparisons of experimentally and naturally weathered alkali feldspars. *Geochim. Cosmochim. Acta* 62, 2771–2788.
- Luo, Y. R. Comprehensive Handbook of Chemical Bond Energies, CRC Press, Boca Raton, FL, 2007.

- Mackie, P.E., and Young, R.A. (1974) Fluorine-chlorine interaction in fluor-chlorapatite. *Journal of Solid-State Chemistry*, 11, 319–329.
- Maher, K., Steefel, C.I., DePaolo, D.J. and Viani, B.E. (2006) The mineral dissolution rate conundrum: Insights from reactive transport modeling of U isotopes and pore fluid chemistry in marine sediments. *Geochimica Et Cosmochimica Acta* 70, 337-363.
- Michel, F. M., J. D. Rimstidt and K. Kletetschka (2018). 3D Printed Mixed Flow Reactor for Geochemical Rate Measurements. *Applied Geochemistry* 89: 86-91.
- Muir, I.J., Bancroft, G.M. and Nesbitt, H.W. (1989) Characteristics of Altered Labradorite Surfaces by SIM and XPS. *Geochimica Et Cosmochimica Acta* 53, 1235-1241.
- Nejad,Z.D., Jung, M. C., and Kim, K.-H. (2018). Remediation of soils contaminated with heavy metals with an emphasis on immobilization technology. *Environmental Geochemistry and Health*, 40(3), 927-953.
- Noiriell, C., Steefel, C.I., Yang, L. and Ajo-Franklin, J. (2012) Upscaling calcium carbonate precipitation rates from pore to continuum scale. *Chemical Geology* 318, 60-74.
- Oelkers, E.H. and Valsami-Jones, E (2008). Phosphate Mineral Reactivity and Global Sustainability. *Elements* 4(2): 83-87.
- O'Neil, J.R. and Taylor, H.P.J. (1967) The oxygen isotope and cation exchange chemistry of feldspars. *American Mineralogist* 52, 1414-1437.
- Parsons, I., Lee, M. R., & Smith, J. V. (1998). Biochemical evolution II: Origin of life in tubular microstructures on weathered feldspar surfaces. *Proceedings of the National Academy of Sciences*, 95(26), 15173
- Pasek, M. A., and Kee, T. P., (2011) On the Origin of Phosphorylated Biomolecules, *Origins of Life: The Primal Self-Organization*, Springer, p. 57-84.
- Petit, J.C., Dran, J.C., Paccagnella, A. and Dellamea, G. (1989) Structural Dependence of Crystalline Silicate Hydration During Aqueous Dissolution. *Earth and Planetary Science Letters* 93, 292-298.
- Putnis A (2002) Mineral replacement reactions: from macroscopic observations to microscopic mechanisms *Mineral Mag* 66:689–708
- Putnis, A., & Putnis, C. V. (2007). The mechanism of reequilibration of solids in the presence of a fluid phase. *Journal of Solid-State Chemistry*, 180(5), 1783-1786.
- Putnis, A. (2014) Why Mineral Interfaces Matter. *Science* 343, 1441-1442.
- Putnis, A. (2015) Sharpened interface. *Nature Materials* 14, 261-262.

- Putnis, A. (2016) Control of silicate weathering by interface-coupled dissolution-precipitation processes at the mineral-solution interface. *Geology* 44, 567-570.
- Putnis, C.V. and Ruiz-Agudo, E. (2013) *The Mineral-Water Interface: Where Minerals React with the Environment*. *Elements* 9, 177-182.
- Rakovan, J. (2002). "Growth and Surface Properties of Apatite." *Reviews in Mineralogy and Geochemistry* 48(1): 51-86.
- Reis, F.D.A.A. (2015) Modeling the growth of an altered layer in mineral weathering. *Geochimica Et Cosmochimica Acta* 166, 298-311.
- Rigali, Mark J., Brady, Patrick V., & Moore, Robert C.. *Radionuclide removal by apatite*. United States. doi:10.2138/am-2016-5769.
- Robie R. A., Hemingway B. S., and Fisher J. R. (1979) Thermodynamic properties of minerals and related substances at 298.15K and 1 bar (105 Pascals) pressure and at higher temperatures: U.S.G.S. Bull. 1452 (with corrections). 1452, 1456p.
- Powner, M. W., Gerland, B., and Sutherland, J. D. (2009) Synthesis of activated pyrimidine ribonucleotides in prebiotically plausible conditions: *Nature*, v. 459, no. 7244, p. 239-242
- Ruiz-Agudo, E., King, H.E., Patino-Lopez, L.D., Putnis, C.V., Geisler, T., Rodriguez-Navarro, C. and Putnis, A. (2016) Control of silicate weathering by interface-coupled dissolution precipitation processes at the mineral-solution interface. *Geology* 44, 567-570.
- Ruiz-Agudo, E., Putnis, C.V. and Putnis, A. (2014) Coupled dissolution and precipitation at mineral-fluid interfaces. *Chemical Geology* 383, 132-146.
- Ruiz-Agudo, E., Putnis, C.V., Rodriguez-Navarro, C., Putnis, A., 2012. Mechanism of leached layer formation during chemical weathering of silicate minerals. *Geology* 40, 947-950.
- Saldi, G.D., Daval, D., Guo, H., Guyot, F., Bernard, S., Le Guillou, C., Davis, J.A., Knauss, K.G., 2015. Mineralogical evolution of Fe-Si-rich layers at the olivine-water interface during carbonation reactions. *Am. Mineral.* 100, 2655-2669.
- Schaad Ph., Poumier F., Voegel J. C., and Gramain Ph. (1997) Analysis of calcium hydroxyapatite dissolution in non-stoichiometric solutions. *Coll. Surf. A: Physicochem. Eng. Asp.* **121**, 217-228.
- Schneider, C. A.; Rasband, W. S. & Eliceiri, K. W. (2012), "NIH Image to ImageJ: 25 years of image analysis", *Nature methods* **9(7)**: 671-675.
- Schwartz, A. W., (2006) Phosphorus in Prebiotic Chemistry: *Philosophical Transactions: Biological Sciences*, v. 361, no. 1474, p. 1743-1749.

- Schweda, P., Sjöberg, L. and Sodervall, U. (1997) Near-surface composition of acid-leached labradorite investigated by SIMS. *Geochimica Et Cosmochimica Acta* 61, 1985-1994.
- Sheldrick, G. (2008) A short history of SHELX. *Acta Crystallographica Section A*, 64(1), 112-122.
- Steeffel, C.I., Appelo, C.A.J., Arora, B., Jacques, D., Kalbacher, T., Kolditz, O., Lagneau, V., Lichtner, P.C., Mayer, K.U., Meeussen, J.C.L., Molins, S., Moulton, D., Shao, H., Simunek, J., Spycher, N., Yabusaki, S.B. and Yeh, G.T. (2015a) Reactive transport codes for subsurface environmental simulation. *Computational Geosciences* 19, 445-478.
- Steeffel, C.I., DePaolo, D.J. and Lichtner, P.C. (2005) Reactive transport modeling: An essential tool and a new research approach for the Earth sciences. *Earth and Planetary Science Letters* 240, 539-558.
- Stock, M. J., Humphreys, M. C. S., Smith, V. C., Johnson, R. D., Pyle, D. M., & EIMF. (2015). New constraints on electron-beam induced halogen migration in apatite†. *American Mineralogist*, 100(1), 281-293. *American Mineralogist*
- Stormer, J.C., Pierson, M.L., and Tacker, R.C. (1993) Variation of F and Cl X-ray intensity due to anisotropic diffusion in apatite during electron microprobe analysis. *American Mineralogist*, 78, 641–648.
- Valsami-Jones, E., Ragnarsdóttir, K.V., Putnis, A., Bosbach, D., Kemp, A.J. and Cressey, G. (1998) The dissolution of apatite in the presence of aqueous metal cations at pH 2-7. *Chemical Geology* 151, 215-233.
- Vogel, G. L., Carey, C. M., Chow, L. C., Gregory, T. M., & Brown, W. E. (1987). Ultramicro Analysis of the Fluid in Human Enamel During in vitro Caries Attack by Hydrochloric Acid. *Caries Research*, 21(4), 310-325.
- Wang, Y., Zhang, L., Hu, M., Liu, H., Wen, W., Xiao, H., & Niu, Y. (2008). Synthesis and characterization of collagen-chitosan-hydroxyapatite artificial bone matrix. *86A*(1), 244-252.
- White, A.F. and Brantley, S.L. (2003) The effect of time on the weathering of silicate minerals: why do weathering rates differ in the laboratory and field? *Chemical Geology* 202, 479- 506.
- Wild, B., Daval, D., Guyot, F., Knauss, K.G., Pollet-Villard, M., Imfeld, G., 2016. pH-dependent control of feldspar dissolution rate by surface altered layers. *Chem. Geol.* 442, 148–159.

- Wirth, R., 2004. Focused Ion Beam (FIB): a novel technology for advanced application of micro- and nanoanalysis in geosciences and applied mineralogy. *European Journal of Mineralogy* 16, 863–876.
- Wirth, R., 2009. Focused Ion Beam (FIB) combined with SEM and TEM: advanced analytical tools for studies of chemical composition, microstructure and crystal structure in geomaterials on a nanometre scale. *Chemical Geology* 261, 217–229.
- Yang, Y.-H., Wu, F.-Y., Yang, J.-H., Chew, D. M., Xie, L.-W., Chu, Z.-Y., Huang, C. (2014). Sr and Nd isotopic compositions of apatite reference materials used in U–Th–Pb geochronology. *Chemical Geology*, 385, 35-55.
- Young, R.A., van der Lugt, W., and Elliott, J.C. (1969) Mechanism for fluorine inhibition of diffusion in hydroxyapatite. *Nature*, 223, 729–730.
- Zhu, Y., Zhang X., Chen Y., Xie Q., Lan J., Qian M., He N., (2009). "A comparative study on the dissolution and solubility of hydroxylapatite and fluorapatite at 25°C and 45°C." *Chemical Geology* 268(1): 89-96.

## Appendix A: Detailed HRTEM-EDX and EELS Methods

Electron transparent cross-sections of HAP and FAP were prepared by focused ion beam milling (FIB) using a FEI Quanta 3D FEG at Johnson Space Center, Houston TX and a FEI Helios 600 NanoLab at NanoEarth Virginia Tech, Blacksburg VA, Respectively.

The HAP cross-section was imaged at 200 kV using the JEM 2500SE TEM, at high resolution using conventional TEM mode. The FIB section showed the presence of a thick protective layer of Carbon (~100 nm). The sample was oriented perpendicular with respect to the c-axis, where excellent diffraction patterns were observed. In some cases, the sample was tilted 10° to give better contrast to the amorphous layer.

The lattice fringes end abruptly at the SAL. In some cases, some vestiges of an ordered linear structure within the SAL close to the interface were observed. This is likely an artifact created during analysis due to inclined interface with respect to beam or delocalization. Overall, the lattice fringes were observed in detail.

The HAP cross-section was chemically mapped using EDS. Two chemical maps were obtained at 1,000,000 and 1,200,000x magnification using a 1-nm probe size, with 0.89 nm spacing between pixels (image pixel resolution of 64 x 50). The maps that were generated concerned the elements O, Ca, P, Ga, and C. Ga was mostly contained by the C coating. To the naked eye, the very thin SAL (5-10 nm) did not show a different chemistry than the rest of the samples (with respect to the chemical maps). However, line profiles obtained from the maps showed the chemical differences between the crystalline HAP and the SAL.

The FAP cross-section was imaged at 200 kV using a FEI TITAN 300 TEM high resolution images were taken in conventional TEM mode with a point resolution of 0.26 nm and Scanning TEM- High Angle Annular Dark Field Mode (STEM-HAADF) with a point-resolution of 0.17 nm. EELS profiles were acquired using a Gatan Model 863 Tridiem GIF (2k x 2k UltraScan 1000FT CCD) in STEM-HAADF mode with an accelerated voltage of 300 kV. FAP FIB section for each area EELS were measurements were taken for Ca L<sub>2,3</sub>, O K and P K. This was performed in continuous mode with a collection semi-angle of 100.0 mrad and an energy dispersion of 0.3 eV/channel). Each measurement had an exposure time of approximately 0.5 seconds to mitigate electron irradiation. This was performed in continuous mode with a collection semi-angle of 100.0 mrad and an energy dispersion of 0.3 eV/channel. EELS Spectra measured had a distortion of < 1.75% and chromaticity of < 1.5 um/eV with a deviation from perfect isochromaticity of < 1.25 eV in magnitude over the entire image field.

The crystalline character of the material was also determined by Selected Area Electron Diffraction (SAED). The lattice fringes were observed in detail, ending abruptly at the SAL. Additionally, faint diffraction spots in the SAED image taken in the SAL are thought to be an artifact created during analysis due to an inclined interface with respect to beam or delocalization.